Accepted Manuscript

Effect of nano-structural properties of biomimetic hydroxyapatite on osteoimmunomodulation

Joanna M. Sadowska, Fei Wei, Jia Guo, Jordi Guillem-Marti, Maria-Pau Ginebra, Yin Xiao

PII: S0142-9612(18)30549-0

DOI: 10.1016/j.biomaterials.2018.07.058

Reference: JBMT 18801

To appear in: *Biomaterials*

Received Date: 20 April 2018

Revised Date: 22 July 2018

Accepted Date: 28 July 2018

Please cite this article as: Sadowska JM, Wei F, Guo J, Guillem-Marti J, Ginebra M-P, Xiao Y, Effect of nano-structural properties of biomimetic hydroxyapatite on osteoimmunomodulation, *Biomaterials* (2018), doi: 10.1016/j.biomaterials.2018.07.058.

Effect of nano-structural properties of biomimetic hydroxyapatite on osteoimmunomodulation.

Joanna M. Sadowska[1,2], Fei Wei[3], Jia Guo[4], Jordi Guillem-Marti[1,2], Maria-Pau Ginebra[1,2,5], Yin Xiao[3]**

[1]Biomaterials, Biomechanics and Tissue Engineering Group, Department of Materials Science and Metallurgical Engineering, Universitat Politècnica de Catalunya (UPC), Av. Eduard Maristany 16, 08019 Barcelona, Spain.

[2]Barcelona Research Centre in Multiscale Science and Engineering, Universitat Politècnica de Catalunya (UPC), Av. Eduard Maristany 16, 08019 Barcelona, Spain.

[3]Institute of Health and Biomedical Innovation and the Australia-China Centre for Tissue Engineering and Regenerative Medicine (ACCTERM), Queensland University of Technology, Brisbane, QLD 4059, Australia

[4]Guanghua School of Stomatology, Hospital of Stomatology, Sun Yat-sen University and Guanghua Provincial Key Laboratory of Stomatology, Guangzhou, Guangdong, 510055, People's Republic of China

[5]Institute for Bioengineering of Catalonia (IBEC), The Barcelona Institute of Science and Technology, Baldiri Reixac 10-12, 08028 Barcelona Spain.

ABSTRACT. *Immune cells are sensitive to the microstructural and textural properties of materials. Tuning the structural features of synthetic bone grafts could be a valuable*

strategy to regulate the specific response of the immune system, which in turn modulates the activity of bone cells. The aim of this study was to analyse the effect of the structural characteristics of biomimetic calcium deficient hydroxyapatite (CDHA) on the innate immune response of macrophages and the subsequent impact on osteogenesis and osteoclastogenesis. Murine RAW 264.7 cells were cultured, under standard and inflammatory conditions, on chemically identical CDHA substrates that varied in microstructure and porosity. The impact on osteogenesis was evaluated by incubating osteoblastic cells (SaOS-2) with RAW- CDHA conditioned extracts. The results showed that macrophages were sensitive to different textural and structural properties of CDHA. Under standard conditions, the impact of inflammatory cytokine production by CDHA played a significant role in the degradation of CDHA, suggesting the impact of resorptive behaviour of RAW cells on biomimetic surfaces. Osteoblast differentiation was stimulated by the conditioned media collected from RAW cells cultured on needle-like nanostructured CDHA. The results demonstrated that needle-like nanostructured CDHA was able to generate a favourable osteoimmune environment to regulate osteoblast differentiation and osteogenesis. Under inflammatory conditions, the incubation of RAW cells with less porous CDHA resulted in a decreased gene expression and release of pro-inflammatory cytokines.

KEYWORDS: *calcium phosphates, biomimetic hydroxyapatite, osteoimmunomodulation, inflammation, osteogenesis, osteoclastogesis*

1. INTRODUCTION

Multiple processes occur during bone healing following the surgical placement of a synthetic bone graft. Among them, immune reactions play an important role in determining

the fate of the implant. The exogenous nature of biomaterials is recognized by the host as a foreign body, which usually triggers the release of cytokines and chemo-attractants by immune cells.[1] The osteoimmune environment generated at the vicinity of the bone graft by these regulatory molecules is of paramount importance, because it can lead to two opposite scenarios. In adverse conditions, it will lead to persistent excessive inflammation. On the contrary, in a favourable environment it will contribute to the regeneration of the bone tissue.

Among all immune cells, macrophages have attracted much interest due to their regulatory role in innate immune response and great plasticity in cellular polarization. In response to various stimuli, macrophages can polarize to pro-inflammatory M1 or anti-inflammatory M2 phenotypes.[2] Moreover, the polarization process is generally accompanied with changes in cell morphology, the release of inflammatory cytokines, and the production of reactive nitrogen and oxygen species.[1,3–6] For instance, the activation into M1 phenotype is characterised by the expression of pro-inflammatory cytokines such as tumour necrosis factor alpha (TNFα), interleukin 6 (IL-6) and interleukin 1 beta (IL-1β).[7,8] In contrast, polarized M2 macrophages produce anti-inflammatory cytokines, mainly interleukin 4 (IL 4), interleukin 10 (IL-10) and interleukin 13 (IL 13) accompanied with high expression of mannose receptors (CD163, CD206).[9]

This inflammatory microenvironment created by M1 and/or M2 immune cells was reported to greatly modulate bone healing events. The pro- inflammatory signals are recognised to stimulate osteoclastic response[10] and mesenchymal stem cell (MSCs) differentiation.[10–12] However, the prolonged exposure to these molecules will lead to chronic inflammation. In turn, the M2 profile participates in osteogenesis and angiogenesis through release of

molecules such as bone morphogenetic protein-2 (BMP-2) or vascular endothelial growth factor (VEGF).[13,14] This intimate relation between immune cells and bone cells highlights the need for better monitoring of the initial stages after biomaterial implantation, redefining the requirements that a bone graft should meet. Hence, to trigger bone regeneration a bone graft should induce a favourable immune environment that results in the appropriate balance between osteogenesis and osteoclastogenesis.[1,15,16]

The response of immune cells is known to be influenced by various factors including topography[17–21], chemistry[16,22–26], porosity[27,28] or stiffness[29–31]. The plasticity of macrophages to switch the phenotype in response to subtle changes opens the door to potential strategies in the development of bone substitutes with osteoimmunomodulatory properties. Hence, modulating the physicochemical features of implants will likely induce various cytokine release profile from immune cells, eliciting different effects on bone dynamics.

Calcium phosphate (CaPs) materials are interesting bone substitutes due to their close chemical resemblance to mineral phase of bone and osteoinductive/ osteoconductive properties. Although countless studies have been devoted to the characterisation of their osteogenic and osteoindutive properties, little attention has been paid to their osteoimmunomodulatory properties. Only recently Chen et al. shed light on the osteoimmunomodulatory features of some CaPs, particularly sintered βtricalcium phosphate (βTCP) ceramics.[15,16,32]

On another hand, it has been recently shown, using model surfaces, that nanotopography also plays a vital role in regulating immune responses.[21,33] In this context, Xiao et al. proposed the concept of "nano-osteoimmunomodulation" as a strategy for the development

of nanotopographies with osteoimmunomodulatory properties, able to regulate bone dynamics.[6]

In this work, we intend to combine both concepts, taking advantage of the possibility to control the nanostructural features of calcium deficient hydroxyapatite (CDHA) materials using biomimetic processing routes. Hence, we investigated the effect of different nanostructures of biomimetic CDHA on osteoimmunomodulation by unravelling the role that surface nanotopography and porosity of CDHA play on the production of inflammatory cytokines and osteoclastic differentiation, as well as the effect of the immune environment created by macrophages cultured on CDHA substrates on the osteogenic differentiation of osteoblasts.

2. MATERIALS AND METHODS

2.1. Synthesis and characterisation of CDHA substrates

CDHA discs were prepared by the self-setting reaction of an hydraulic paste of α tricalcium phosphate (αTCP) powder at 37°C, described in a previous work.[34] αTCP was obtained by sintering a 1:2 molar mixture of calcium hydrogen phosphate ($CaHPO_4$, Sigma-Aldrich, St. Louis, USA) and calcium carbonate ($CaCO_3$, Sigma-Aldrich, St. Louis, USA) at 1400°C for 15 h and subsequent quenching in air.

In previous studies we showed that it was possible to tune the textural properties of the material by modifying the grain size of the starting αTCP powder and the liquid-to-powder ratio of the paste[35], this allowing the preparation of chemically identical CDHA substrates that varied in microstructure, specific surface area and porosity.

Therefore, two milling protocols were applied with the purpose of obtaining the powder with coarse (C: 5.2μm median size) and fine (F: 2.8 μm) particle size.[35] In order to obtain a mouldable paste, the solid phase that consisted of αTCP and 2wt% of precipitated hydroxyapatite (PHA; Merck 2143, Merck, Darmstardt, Germany) was mixed with an aqueous solution containing 2.5wt% of disodium hydrogen phosphate (Na_2HPO_4, Merck, Darmstadt, Germany). The samples were prepared with two different liquid-to-powder (L/P) ratios: 0.35 mL/ g and 0.65 mL/ g, transferred to Teflon moulds (6mm of diameter, 2mm of height) and left to set in water at 37°C for 7 days. The specimens were coded as C35, F35, C65 and F65, where C and F stand for coarse and fine powder respectively and 35 and 65 stand for the liquid to powder ratio of 0.35 and 0.65 ml/g respectively.

The microstructure of the substrates was characterised by Scanning Electron Microscopy (SEM, TESKAN MIRA3) with an acceleration voltage of 5 kV after depositing a thin layer of gold-palladium with EM SC005 Gold Coater (Leica). The surface roughness was characterized by optical interferometry (Veeco Wyko NT1100), using a 50x magnification and a scanned area of 47.5 x 63.4 μm^2. Images were acquired using Vision32 software. For mechanical testing, cylinders of 6 mm of diameter and 12 mm of height were prepared following the same protocol described above. Afterwards, the samples (n=10) were subjected to a compression test at a crosshead speed of 1 mm/ min in a Universal Testing Machine (Adamel Lhomargy DY 34). The Young's modulus was calculated from the linear region of the stress-strain curve.

2.2. Cell culture

Two cell lines, the murine-derived macrophage cell line RAW 264.7 (RAW) and human osteosarcoma cell line SaOS-2, were used in this study. Both cell lines were maintained in

Dulbecco's Modified Eagle Medium (DMEM; Gibco®, Life Technologies Pty Ltd., Australia) supplemented with 10% heat-inactivated fetal calf serum (FCS; In Vitro Technologies, Australia) and 1% (50 U/ml and 50 µg/ml, respectively) penicillin/streptomycin (P/S; Gibco®, Life Technologies Pty Ltd., Australia) at 37°C with a 5% CO_2 humidified atmosphere.

2.3. Osteoimmunomodulatory effect of CDHA on macrophages under standard and inflammatory conditions

The behaviour of macrophages was evaluated after direct exposure to CDHA substrates. For that purpose, the discs were sterilised with 80% ethanol, rinsed thrice with phosphate-buffered saline (PBS, Oxoid) and incubated overnight with complete medium. Subsequently, RAW cells were seeded at a density $7x10^5$/ cm^2 for all experiments unless otherwise stated.

To induce the inflammatory environment 1 µg/ mL of lipopolysaccharide (LPS, Escherichia coli 055:B5, R&D Systems) was added following previous protocols.[8,21] Briefly, after 12 hours of RAW cells seeding, standard medium was replaced with medium containing LPS and incubated for 2 hours. Subsequently, samples were thoroughly washed with PBS, placed in new well plate and incubated following 6 hours in serum starvation medium.

2.3.1. Metabolic activity of RAW cells on CDHA substrates

The metabolic activity of RAW cells under standard conditions, was evaluated at day 1, 3 and 5 trough MTT [3-(4,5- dimethylthiazol-2-yl)-2,5-diphenyl tetrazolium bromide] assay (R&D Systems). Briefly, the samples were washed with PBS and transferred to a new well plate, where 30 µL of 5mg/mL of MTT solution was added to a total volume of 300 µL of DMEM leading to a final concentration of 0.5mg/mL of MTT reagent. After 4 h of

incubation, MTT-DMEM solution was carefully removed and 150 µL of dimethyl sulfoxide (DMSO, Univar USA) was added in order to dissolve formazan crystals. Subsequently, the absorbance was read at 570 nm using microplate spectrophotometer (Benchmark Plus, Tacoma, Washington, USA).

2.3.2. Cell morphology

The morphology of RAW cells on CDHA substrates was observed at day 1 and 3 for standard conditions and 6 hours after incubation with LPS for inflammatory conditions. Images were acquired by SEM (TESKAN MIRA3) using an acceleration voltage of 5 kV, and by confocal microscopy (CLSM, Nikon A1).

For SEM visualisation, cells were thoroughly washed with PBS and subsequently fixed with 3% glutaraldehyde. Samples were then rinsed with PBS and post- fixed with 1% osmium tetraoxide incubation for 1h. The process was followed by dehydration through consecutive washings with increasing concentrations of ethanol solution (50%, 70%, 90%, 100%) achieving a complete dehydration in hexamethyldisilazane (HMDS, Sigma-Aldrich). Prior to visualisation, the discs were covered with a gold thin layer using EM SC005 Gold Coater (Leica).

For confocal microscopy, the cells were washed with PBS and fixed with 4% paraformaldehyde solution (PFA, Sigma-Aldrich). The membrane permeabilization was carried out through incubation with 0.1 % Triton X- 100 (Merck) in PBS during 15 min. For nitric oxide synthase (iNOS) staining, RAW cells were additionally incubated for 1h with blocking solution consisting of 1% bovine serum albumin (BSA, Sigma-Aldrich) in PBS followed by 1 h incubation with primary and secondary antibodies, rabbit polyclonal iNOS in 1% BSA (1:100, Abcam) and Alexa Fluor488 Conjugate anti-rabbit IgG in 0.1%

Triton X-100 in PBS (1:1000, Cell Signaling Technology), respectively. For cytoskeleton and nuclei staining, cells were incubated with Alexa Fluor 594 for 1 h (1:300, Life Technologies Pty Ltd., Australia) and 4, 6-diamidino-2-phenylindole (DAPI) (1:1000, Molecular Probes) for 2 min, both in 0.1 % Triton X- 100 in PBS solution. Between all steps, three rinses for 5 minutes with 0.15% glycine in PBS were performed. Images were acquired using LASX software and processed using Fiji/Image-J package. Additionally, image analysis was performed in order to quantify the spreading area and elongation ratio (n=50) of macrophages.

2.3.3. Response of RAW cells to CDHA substrates

For standard conditions, RAW cells were seeded at a density of $7x10^5$cells/ cm^2. After 6 hours of incubation the cell culture medium was replaced with serum free medium and the cells were incubated for additional 6 hours. Then, the substrate-conditioned medium (CM) was recovered for further experiments being stored at -80^{o}C. For RNA extraction, samples were washed with PBS and total RNA from cells was extracted applying TRIzol reagent (Ambion^{TM}, Life Technologies Pty Ltd., Australia) following manufacturer instructions. Subsequently, the concentration of total RNA was quantified by NanoDrop ND-1000 spectophotometer (NanoDrop technologies, Motchanin, DE, USA) and one thousand nanograms of total RNA were used for synthesis of complementary DNA using DyNAmo™ cDNA Synthesis Kit (Genesearch, QLD, Australia). Detection of inflammatory genes expression (IL-1β, IL-6, TNFα, iNOS, IL-10, CD206) was performed with a QuantstudioTM Real-Time PCR machine (Applied Biosystems, Foster City, California, USA) using SYBR Green qPCR Master Mix (Life Technologies). In all RT-qPCR runs, the specificity of primers was determined by melt curves analysis. The raw values were, then, expressed as relative fold applying the $2^{-\Delta\Delta Ct}$ method where $\Delta\Delta Ct$= (Ct_{sample} (gene of interest) - Ct_{sample}

(endogenous reference gene)) – (Ct_{TCPS} (gene of interest) – Ct_{TCPS} (housekeeping gene)) and Ct represents the cycle threshold of sample [36]. The 18S ribosomal RNA gene expression was used as endogenous reference gene and the RAW cells cultured on TCPS condition were used for normalizing RT-qPCR data. The list of primers used for RT-qPCR experiments is specified in Table 1.

Table 1. *Primers' sequences used in this study*

Gene	Gene symbol	Primer' sequences (5' to 3')
18S ribosomal RNA	*18S*	*F:CGGAACTGAGGCCATGATTAAG* *R:GTATCTGATCGTCTTCGAACCTCC*
Interleukin 1 beta	*Il-1β*	*F:TGGAGAGTGTGGATCCCAAG* *R:GGTGCTGATGTACCAGTTGG*
Interleukin 6	*Il-6*	*F:ATAGTCCTTCCTACCCCAATTTCC* *R:GATGAATTGGATGGTCTTGGTCC*
Tumor necrosis factor alpha	*Tnfa*	*F:CTGAACTTCGGGGTGATCGG* *R:GGCTTGTCACTCGAATTTTGAGA*
Nitric oxide synthase	*inos*	*F:CACCAAGCTGAACTTGAGCG* *R:CGTGGCTTTGGGCTCCTC*
Oncostatin M	*Osm*	*F:ACGGTCCACTACAACACCAG* *R:CCATCGTCCCATTCCCTGAAG*
Transforming growth factor beta 1	*Tgfβ1*	*F:CAGTACAGCAAGGTCCTTGC* *R:ACGTAGTAGACGATGGGCAG*

Vascular endotelial growth factor A	*Vegf a*	*F:GTCCCATGAAGTGATCAAGTTC* *R:TCTGCATGGTGATGTTGCTCTCTG*
Cathepsin K	*Ctsk*	*F:CCAGTTTTACAGCAGAGGTGTG* *R:CTTGCTTCCCTTCTGGGTG*
Carbonic anhydrase 2	*Car2*	*F:AGCAGCGAGCAGATGTCTC* *R:TGAGCTGGACGCCAGTTG*
Matrix metallopeptidase 9	*Mmp9*	*F:GGGCGTGTCTGGAGATTCG* *R:CACCTGGTTCACCTCATGGTC*
Interleukin 10	*Il-10*	*F:CAGGACTTTAAGGGTTACTTG* *R:ATTTTCACAGGGGAGAAATC*
Mannose receptor C type	*Cd206*	*F:AGACGAAATCCCTGCTACTG* *R:CACCCATTCGAAGGCATTC*
Runt-related transcription factor 2	*Runx2*	*F:GACGAGGCAAGAGTTTCACC* *R:ATGAAATGCTTGGGAACTGC*
Bone morphogenic protein 2	*BMP-2*	*F:TGCCATTGTTCAGACGTTGG* *R:GTACTAGCGACACCCACAAC*
Bone sialoprotein	*BSP*	*F:TTTCTGCTACAACACTGGGCTATG* *R:TTGTTATATCCCCAGCCTTCTTG*
Osteocalcin	*OCN*	*F:GCAAAGGTGCAGCCTTTGTG* *R:GGCTCCCAGCCATTGATACAG*
Collagen type I	*COLL I*	*F:AGAACAGCGTGGCCT* *R:TCCGGTGTGACTCGT*

The same procedures were applied for extraction of the RNA and evaluation of the gene expression of RAW cells exposed to an inflammatory environment (after LPS stimulation, as explained in section 2.3. Additionally, cytokine release was analysed using enzyme-linked immunosorbent assay (ELISA). For that purpose, the supernatants were evaluated for the presence of IL-6 and TNF-α using a mouse IL-6 Uncoated ELISA kit and a mouse TNF-α Uncoated ELISA kit, respectively (Invitrogen). The different time points for the evaluation of the inflammatory response of RAW cells, either with or without LPS stimulation, were chosen based on previous studies where the adequate time points for detection of cytokine release and gene expression were determined.[8,16]

2.3.4. Osteogenic and osteoclastogenic activity of macrophages

The osteogenic and osteoclastogenic activity of RAW cells was determined through detection of specific genes (osteogenesis: OSM, TGFβ and VEGF; osteoclastogenesis: CTSK, CAR2, MMP9) following the specific time points and protocols detailed in section 2.3.3. The primers' sequences are those displayed in Table 1.

To assess cell morphology and substrate degradation, SEM images were acquired at day 3, following the fixation and visualisation protocols described in section 2.3.2. Moreover, the CDHA discs were incubated in complete DMEM without the presence of RAW cells and the microstructure of the substrates was evaluated after 3 days by SEM (Zeiss Neon 40, Oberkochen, Germany), in order to discern any physic-chemical degradation from the potential degradation caused by cellular activity.

The ionic concentrations of Ca^{2+} and P_i of cell culture media with and without cells was quantified by inductively coupled plasma-optical emission spectrometry (ICP-OES, Perkin Elmer, MA, USA). The ionic concentration was determined at day 1 and 3 for standard

conditions. Prior to quantification, the cell culture medium was diluted 5-fold with 2% of ultrapure nitric acid (Sigma-Aldrich).

2.4. The effect of the supernatant of RAW cells cultured on the CDHA substrate on the osteogenic differentiation of SaOS-2 cells

In order to investigate the effect of the osteoimmune environment created by the macrophages cultured onto the substrate, SaOS-2 cells were incubated with CM from section 2.3.3, under standard and inflammatory conditions. For all experiments, except where otherwise stated, SaOS-2 cells were plated on TCPS at a density of $2.5x10^4$ cells/ cm^2. After 24h the standard medium was replaced with RAW- substrate CM with 10% of FCS and SaOS-2 cells were incubated for up to 3 days. Cells cultured with standard DMEM medium were used as a control.

2.4.1. Osteogenic- related gene expression and protein secretion by SaOS-2 cells

The bone-related gene expression was quantified through RT-qPCR at day 3 of cell culture. The RNA extraction and RT-pPCR protocols are detailed in section 2.3.3. The relative expressions of Runx2, BMP-2, BSP, OCN and COLL I (Table 2) was determined using comparative Ct ($2^{-\Delta\Delta CT}$) method. 18S gene expression was used as housekeeping gene and SaOS-2 cells cultured on TCPS at day 1, instead of day 3, were used to normalize the data, to ensure that the reference values were not skewed by the osteogenic differentiation promoted by cell confluence at day 3.

The evaluation of protein expression was carried out using Western Blot detection. Briefly, after incubation with CM, cell lysates were collected using RIPA lysis buffer. Subsequently, 20 μg of proteins from each sample were separated on SDS-PAGE gel followed by transfer

onto nitrocellulose membranes (Pall Corporation, East Hills, New York, USA). The membranes were then blocked for 1h in Odyssey blocking buffer (LI-COR Biosciences, Lincoln, Nebraska, USA). Afterwards, the membranes were incubated overnight at 4°C with primary antibodies against ALP, Runx2, COLL I and αtubulin (all 1:1000, rabbit anti-human; Abcam, Cambridge, United Kingdom). The protein bands were visualised using the Odyssey infrared imaging system (LI-COR Biosciences, Lincoln, Nebraska, USA). The relative intensities of protein bands were quantified using Fiji/Image-J package.

For the visualisation of cell morphology, SaOS-2 cells were seeded on glass coverslips placed inside 24-well plate following the seeding and incubation protocols described in section 2.4. Cytoskeleton and nuclei were stained using the immunocytochemistry methods detailed in section 2.3.2. Additionally cells were incubated with rabbit anti-human ALP (1:100, Abacam) followed by Alexa Fluor488 Conjugate anti-rabbit IgG secondary antibody (1:1000, Cell Signaling Technology, Danvers, MA) for ALP staining. The images were acquired using CLSM (Nikon A1) and processed with Fiji/Image-J package.

2.4.2. Mineralization of SaOS-2 cells

For the mineralization assay SaOS-2 cells were seeded at a semi-confluent density of $6x10^4$ cells/ cm^2. After 24h, the medium was replaced with CM combined with osteogenic medium at ratio 1:2. The supplements for osteogenic medium were 50 µg/ mL ascorbic acid, 10 mM β glycerophosphate and 100 nM dexamethasone. The medium was refreshed every third day. At 14 days of culture, SaOS-2 cells were washed with double distilled H_2O (ddH_2O) and fixed with 4% of PFA for 15 min at RT. Afterwards, cells were stained using Alizarin red solution (ARS, Sigma-Aldrich) at pH 4.2 for 20 min. The unbound stain was removed

by various washings with ddH_2O. The images were acquired using a light microscope (Nikon ECLIPSE TS100) after previous air dying of the samples.

2.5. Statistical analysis

All statistical analyses were performed using SPSS software (IBM SPSS, Armonk, NewYork, USA). The data presented in graphs represents mean ± standard deviation (SD) (n=3 unless otherwise stated). Normality was checked through the Saphiro–Wilk test. Statistical differences between groups for non- parametric data were analysed through Mann-Whitney U test. Statistical differences between groups for parametric data were analysed using One-way ANOVA. The homogeneity of variance was assessed using Levene's test. In case of non-significant Levene's test, the Tukey's post hoc test was applied for data analysis. In case of significance, Tamhane's post hoc test was used. The level of significance for all tests was set at $p<0.05$.

3. RESULTS

3.1. Material characterization

The detailed physicochemical characterisation regarding crystalline phases, porosity and pore size distribution and specific surface area (SSA) of the biomimetic CDHA substrates analysed in this study was previously described.[34,37] Table 2 displays the specific surface area and porosity of the CDHA substrates studied.

Table 2. *Roughness, Young's modulus, specific surface area (SSA) and porosity of the biomimetic calcium deficient hydroxyapatite substrates used in this study.*

Substrate	Roughness Ra	Young's	SSA (m^2/g)*[38]*	Porosity

	(μm)	modulus (GPa)		(%)*[38]*
F35	*1.12*± 0.18	*20.40*± 1.80	*24.43*± *0.03*	*34.3*
F65	*1.06*± 0.42	*5.55*± 2.05	*27.32*± 0.02	*53.0*
C35	*1.94*± 0.25	*19.06*± 2.88	*14.11*± 0.01	*33.4*
C65	*1.93*± 0.48	*5.31*± 2.50	*14.42*± 0.01	*54.4*

The microstructure of the fine (F35 and F65) and coarse (C35 and C65) CDHA substrates is displayed in Figure 1. Lower magnification SEM images are displayed in Supplementary Figure 1. All substrates consisted in crystal agglomerates, but whereas the use of fine α TCP particles resulted in needle-like crystals of nanometric size, coarse αTCP particles led to plate-like crystals of micrometric size. Moreover, the different liquid to powder ratios used led to different porosities, and subsequently to different stiffness values. The substrates with low L/P ratio, and therefore lower porosity, presented 4-fold higher Young's modulus, approximately 20 GPa, compared to the 5 GPa presented by the CDHA substrates prepared with high L/P ratio (Supplementary Figure 3).

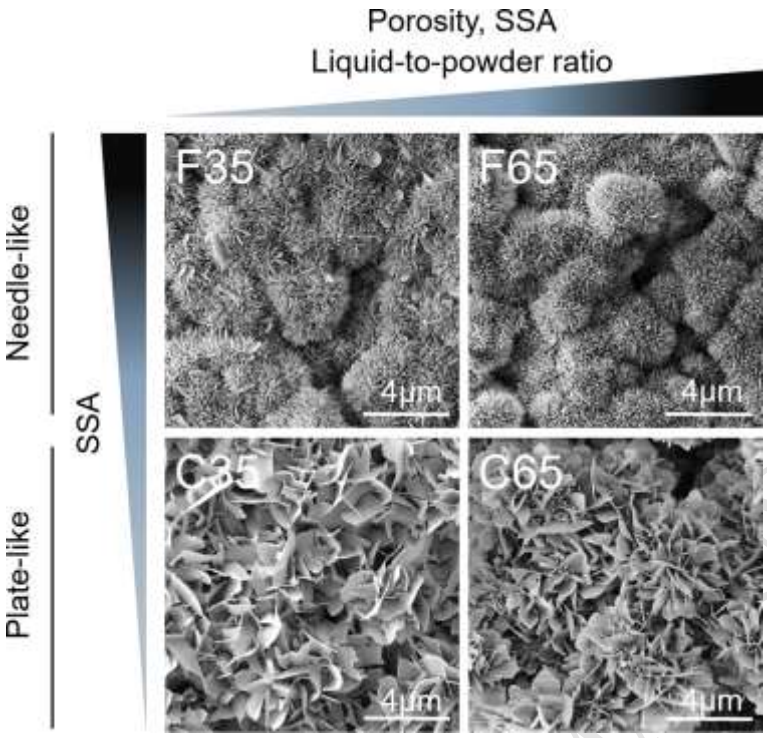

Figure 1. *SEM images of the surface microstructure of CDHA substrates.*

3.2. Effect of CDHA substrates on the response of macrophage RAW cells under standard conditions

3.2.1. RAW cells proliferation and morphology

Similar metabolic activity was observed when RAW cells were cultured on the different CDHA discs for 1,3 and 5 days. The absorbance values at day 3 and 5 in the biomimetic substrates were significantly lower than that of the tissue culture polystyrene (TCPS) control group (Figure 2A).

The macrophages showed predominantly a round morphology in all substrates after 1,3 and 5 days of culture (Figure 2B, Supplementary Figure 4). Moreover, in all conditions cells organized into clusters. Higher spreading of RAW cells on all CDHA was observed at day 1 in comparison to the control group (Figure 2C). At day 3, the cells cultured on F35

and C65 showed significantly different spreading area. Whilst on F35 the cells were less spread, on C65 they were more spread compared to control. At day 5, RAW cells presented lower spreading area in all biomimetic substrates compared to the control. No significant changes of cell elongation ratio were observed (Figure 2D).

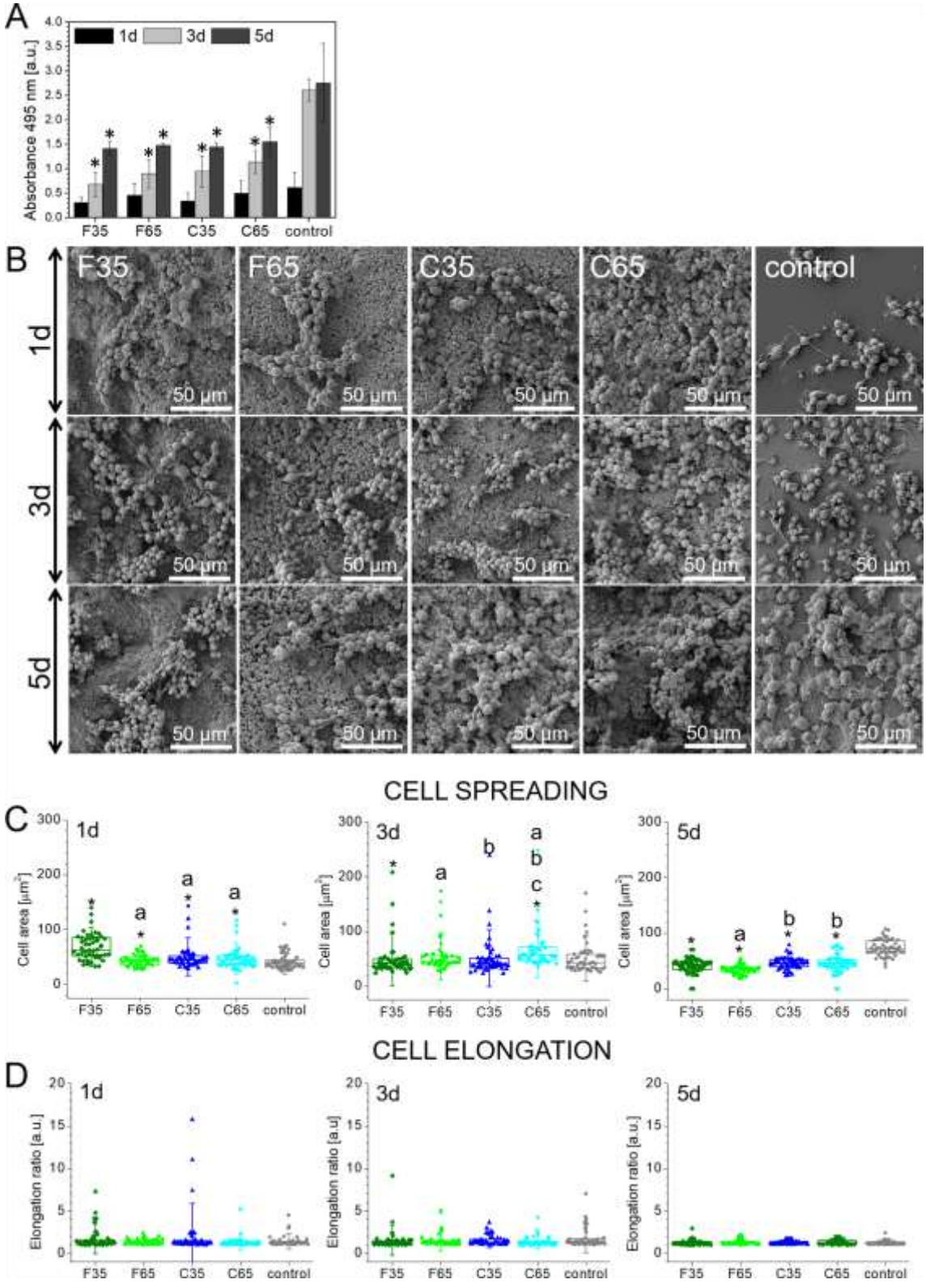
A
Absorbance 495 nm [a.u.]
1d
3d
5d
F35
F65
C35
C65
control
B
F35
F65
C35
C65
control
1d
3d
5d
50 µm
CELL SPREADING
C
1d
3d
5d
Cell area [µm²]
CELL ELONGATION
D
1d
3d
5d
Elongation ratio [a.u.]

Figure 2. A) *Metabolic activity of RAW cells on CDHA substrates at 1, 3 and 5 days of culture, detected by MTT. No significant difference was found between various CDHA substrates.* ***** *Indicates statistically significant differences (P < 0.05) compared to the control TCPS group at the corresponding time point.* **B)** *Morphology of RAW cells observed by SEM on CDHA substrates at 1, 3 and 5 days. RAW cells cultured on glass coverslip were used as a control group.* **C)** *Cell spreading at 1, 3 and 5 days of cell culture.* **D)** *Cell elongation ratio at 1, 3 and 5 days of cell culture. In* **C** *and* **D** *graphs, symbols represent individual cells (n=50), the boxes represent 25th and 75th percentile, the middle line is the median and whiskers are standard deviation.* ***** *Indicates statistically significant difference (P < 0.05) compared to the control group. Statistically significant differences between substrates were indicated with letters (a, b, c) where a, b and c indicates significant difference (P < 0.05) compared to F35, F65 and C35, respectively.*

3.2.2. Inflammatory response of RAW cells

The expression of pro-inflammatory (IL-1β IL-6, TNFα and nitric oxide synthase: iNOS) and anti- inflammatory (IL-10 and CD206) genes by RAW cells cultured on the CDHA was evaluated using RT-qPCR (Figure 3). Overexpression of IL-1β and TNF-α genes was observed for all CDHA substrates compared to TCPS. The upregulation of IL-1β and IL-6 was more pronounced for F35 whilst both C35 and C65 coarse substrates upregulated the expression of TNF-α The gene expression of iNOS and CD206 was lower when RAW cells were cultured on CDHA compared to TCPS. The expression of IL-10 genes was under the detection limit (data not shown).

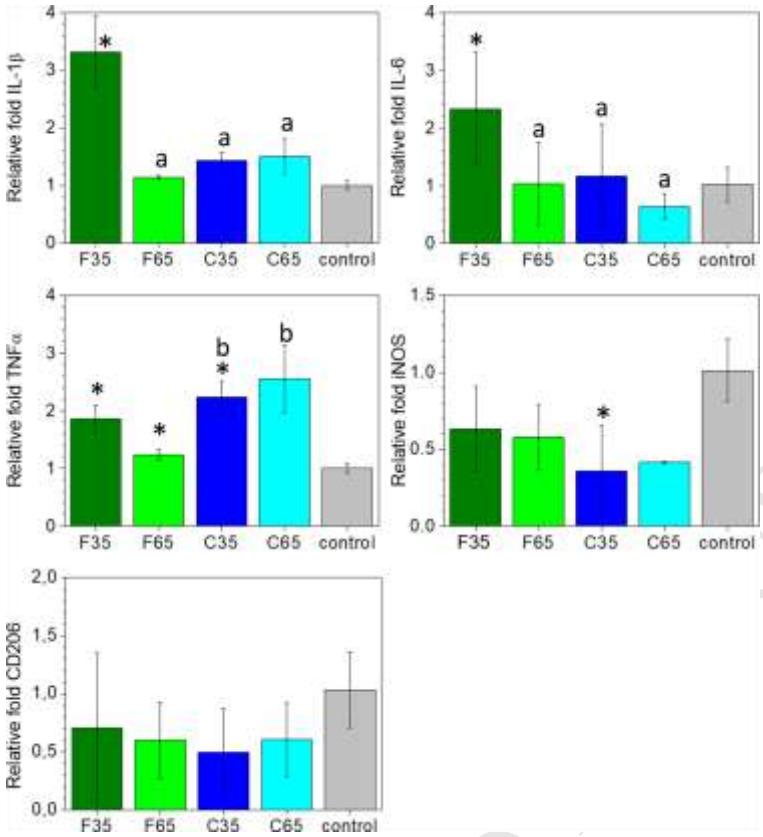

Figure 3. *Relative expressions of inflammation related genes: IL-1β IL-6, TNFα iNOS (pro-inflammatory) and CD206 (anti-inflammatory) of RAW cells cultured on CDHA substrates for 12 h. The values were normalized with respect to housekeeping gene 18S using RAW cells cultured on TCPS as a control sample. * Indicates statistically significant difference (P < 0.05) compared to the control group. Statistically significant differences between substrates were indicated with letters (a, b) where a and b indicate statistically significant differences (P < 0.05) compared to F35 and F65, respectively.*

3.2.3. Osteogenic and osteoclastogenic activity of RAW cells

The gene expression of osteogenic (oncostatin M: OSM, transforming growth factor beta: 1TGFβand VEGF) and osteoglastogenic (cathepsin K: CTSK, carbonic anhydrase 2: CAR2 and matrix metallopeptidase 9: MMP9) markers are depicted in Figure 4A and 4B,

respectively. In general, CDHA substrates showed similar osteogenic gene expression compared to the control except for F35 where lower levels of osteogenesis related markers were observed. Noteworthy, cells cultured on C65 presented higher levels of osteogenic-related markers although only TGF-βgene expression was significantly higher compared to the other substrates. Moreover, C65 substrate also stimulated the gene expression of osteoclastogenic markers, especially for CAR2 and MMP9. Overall, the CDHA with high L/P ratio, F65 and C65, induced higher values of osteogenic and osteoclastogenic markers compared to their low L/P ratio equivalents, F35 and C35, and the same trend was observed when comparing the substrates with low SSA (C35 and C65) with their high SSA (F35 and F65) counterparts, the first inducing a higher expression than the last.

The osteoclastic activity of RAW cells was also studied through visualisation of the morphology of the cells and the underlying substrate (Figure 4C) and measurement of ionic concentrations in the cell culture medium (Figure 4D). Higher magnification SEM images (Figure 4C, right panel) taken at day 3 revealed the presence of degraded crystals of CDHA in the regions near the macrophages compared to pristine needle and plate-like microstructure of the biomaterials. No degradation was observed in CDHA substrates incubated with cell culture medium in absence of RAW cells (Supplementary Figure 3).

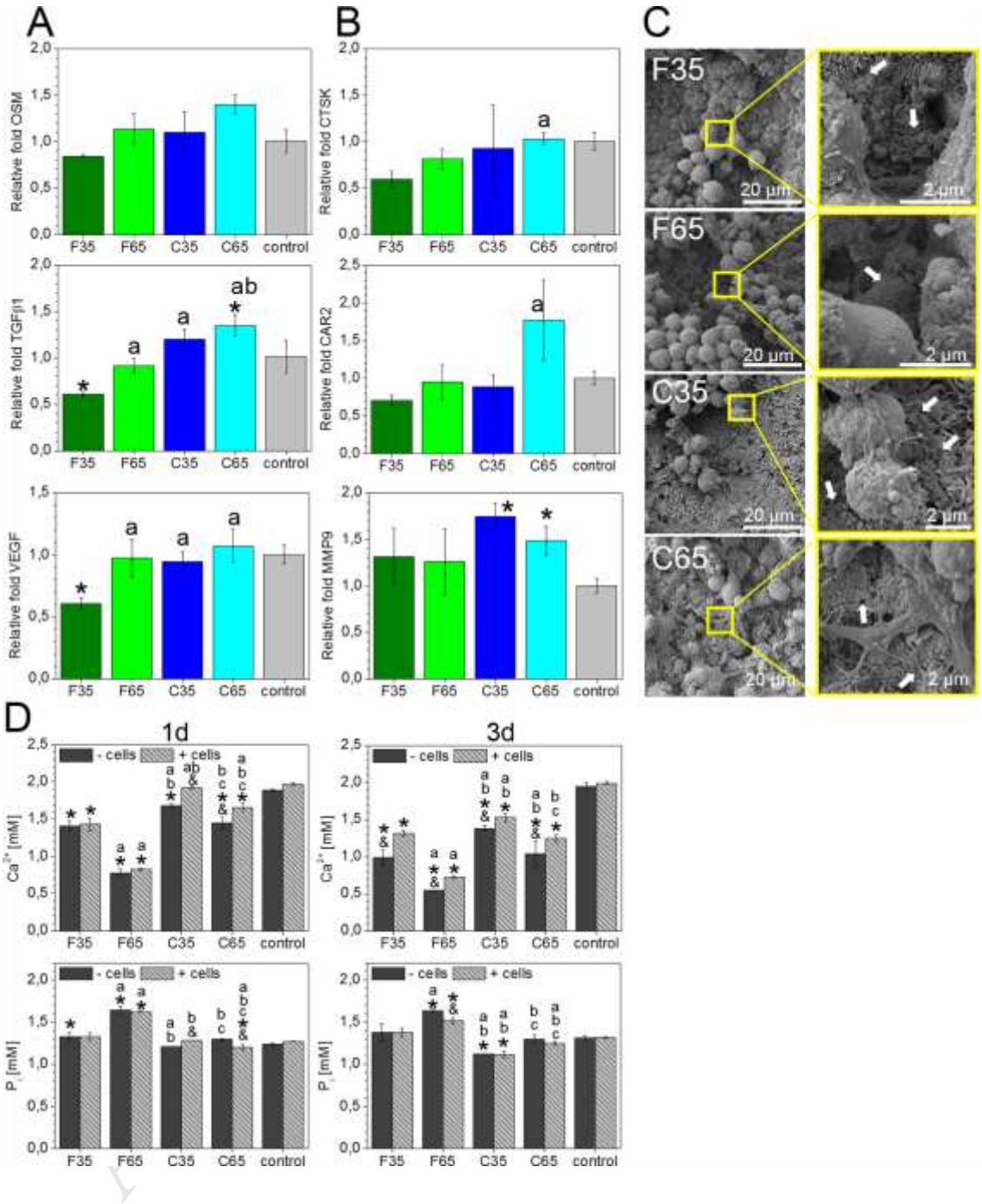

Figure 4. *Osteogenic and osteoclastogenic activity of RAW cells cultured on CDHA substrates for 12 h.* **A)** *Relative expressions of osteogenesis related genes: OSM, TGFβ1 and VEGF.* **B)** *Relative expressions of osteoclastogenesis related genes: CTSK, CAR2, MMP9. In both A and B graphs, the values were normalized with respect to housekeeping*

*gene 18S using RAW cells cultured on TCPS as a control sample. * Indicates statistically significant difference (P < 0.05) compared to the control TCPS group. Statistically significant differences between substrates were indicated with letters (a, b, c) where a, b and c indicate statistically significant differences (P < 0.05) compared to F35, F65 and C35 respectively.* **C)** *SEM images of RAW cells on the CDHA substrates at day 3, showing degraded crystals (white arrows) presumably as a result of cell activity. Left panel: general view, right panel: detailed view.* **D)** *Calcium and phosphate concentrations in the cell culture medium in presence of CDHA, with (patterned columns) or without cells (plain columns), after 1 or 3 days. The ionic concentrations were evaluated for n=2 samples. For each substrate, & indicates statistically significant difference (P < 0.05) between ionic concentration of cell culture medium with or without cells. * Indicates statistically significant difference (P < 0.05) compared to corresponding control group i.e. cell culture medium with or without cells. Statistically significant differences between substrates were indicated with letters (a, b, c) where a, b and c indicates significant difference (P < 0.05) compared to F35, F65 and C35, respectively.*

The concentrations of calcium and phosphate ions in cell culture medium without cells were 1.89± 0.02 mM 1.24± 0.02 mM, respectively. No statistically significant changes of Ca^{2+} *and* P_i *content were observed in presence of cells for TCPS group. In general, the levels of calcium decreased in presence of CDHA compared to TCPS, the decrease being more pronounced for F65. The presence of macrophages counteracted the decrease of* Ca^{2+} *increasing its concentration up to 15% compared to the substrate alone (Figure 4D). This was observed at all time points for C35 and C65, whereas in F substrates the effect was more pronounced at day 3.*

Little alterations of phosphate were noticed. Overall, P_i levels increased only in presence of F CDHA substrates, especially F65. There were no clear trends associated to the presence or absence of cells and phosphate concentration in the cell culture medium (Figure 4D).

3.3. The effect of CDHA and RAW cell conditioned medium on osteogenic differentiation of osteoblastic SaOS-2 cells

To study the effect of the microenvironment created by biomimetic substrates and macrophages on osteogenesis, osteoblast-like SaOS-2 cells were incubated with CDHA-RAW conditioned extracts. SaOS-2 cells were also cultured with conditioned extracts from RAW cells cultured on TCPS, "SaOS-2 control+", and with non-conditioned medium, "SaOS-2 control-".

The expression of the osteogenic markers alkaline phosphatase (ALP), Runt-related transcription factor 2 (Runx2), collagen type I (COLLI), bone morphogenic protein 2 (BMP-2), bone sialoprotein (BSP) and osteocalcin (OCN) was evaluated using RT-qPCR. The results showed an up-regulation of osteogenic-related genes in the cells cultured on the F CDHA substrates, this being especially pronounced for BMP-2, BSP and COLLI, and also for Runx2 and OCN in the case of F65. SaOS-2 cells incubated with extracts from plate-like substrates presented similar gene expression values compared to SaOS-2 control+, except for a decrease observed in the case of BSP (Figure 5A). In general, "SaOS-2 control+" showed slightly higher expression of osteogenic genes compared to "SaOS-2 control-" being statistically significant only for Runx2.

Western blot analyses were performed to evaluate COLLI, Runx2 and ALP protein production. In general, no significant differences were observed between SaOS-2 cells stimulated with RAW extracts (SaOS-2 control+) and non-treated cells (SaOS-2 control-).

Moreover, plate-like CDHA substrates induced lower protein levels compared to needle-like CDHA. Noteworthy, the protein levels of Runx2 and ALP was significantly higher in F35 substrate compared to all the other conditions (Figure 5B).

The mineralization of SaOS-2 cells were assessed through Alizarin Red staining. Calcium deposition and nodule formation was observed to be fostered in the cells cultured in conditioned medium compared to SaOS-2 control- (Figure 5C).

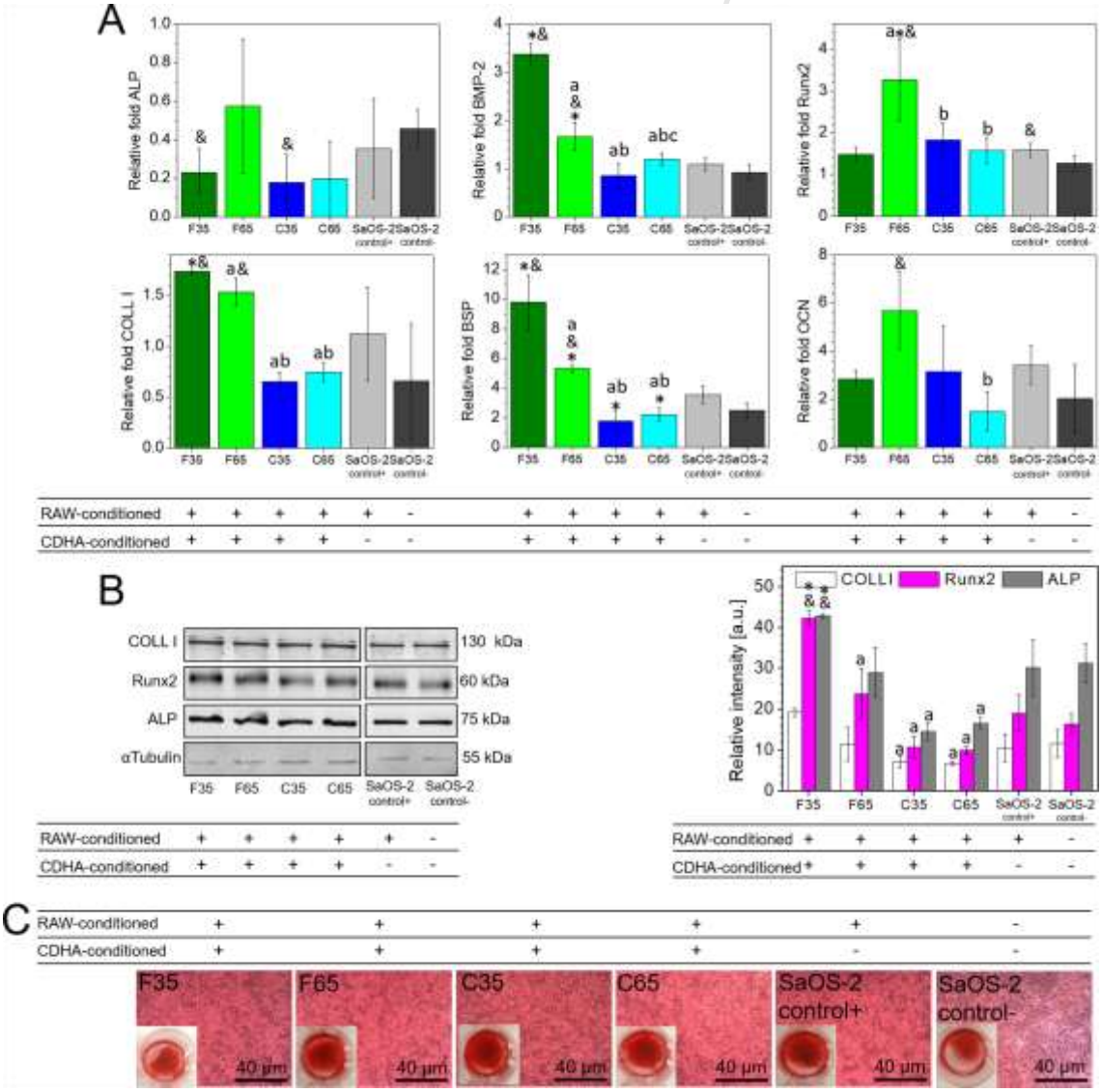

Figure 5. *Effect of CDHA- RAW264.7 conditioned medium on osteogenic activity of SaOS-2 cells.* **A)** *Relative expressions of osteogenesis related genes: ALP, Runx2, BMP-2, BSP, COLL I, OCN.* **B)** *Expression of osteogenesis related proteins (COLL I, Runx2, ALP) detected by Western blot and their relative intensity.* **C)** *Mineralization of SaOS-2 detected through Alizarin Red Staining. In all graphs "SaOS-2 control+" refers to osteoblastic cells stimulated with RAW cells conditioned medium (without CDHA substrate) whilst "SaOS-2 control-" refers to osteoblastic cells in their standard cell culture medium.* ***** *and & indicate statistically significant difference ($P < 0.05$) compared to the SaOS-2 control+ and SaOS-2 control– group, respectively. Statistically significant differences between substrates were indicated with letters (a, b, c) where a, b and c indicate statistically significant differences ($P < 0.05$) compared to F35, F65 and C35 respectively.*

The results of gene and protein expression were also confirmed by visualisation of ALP staining and semiquantitative analysis of images. Overall, osteoblastic cells incubated on RAW extracts from fine CDHA presented more intense ALP staining compared to controls or coarse substrates, being significantly higher for F35 (Figure 6A and B).

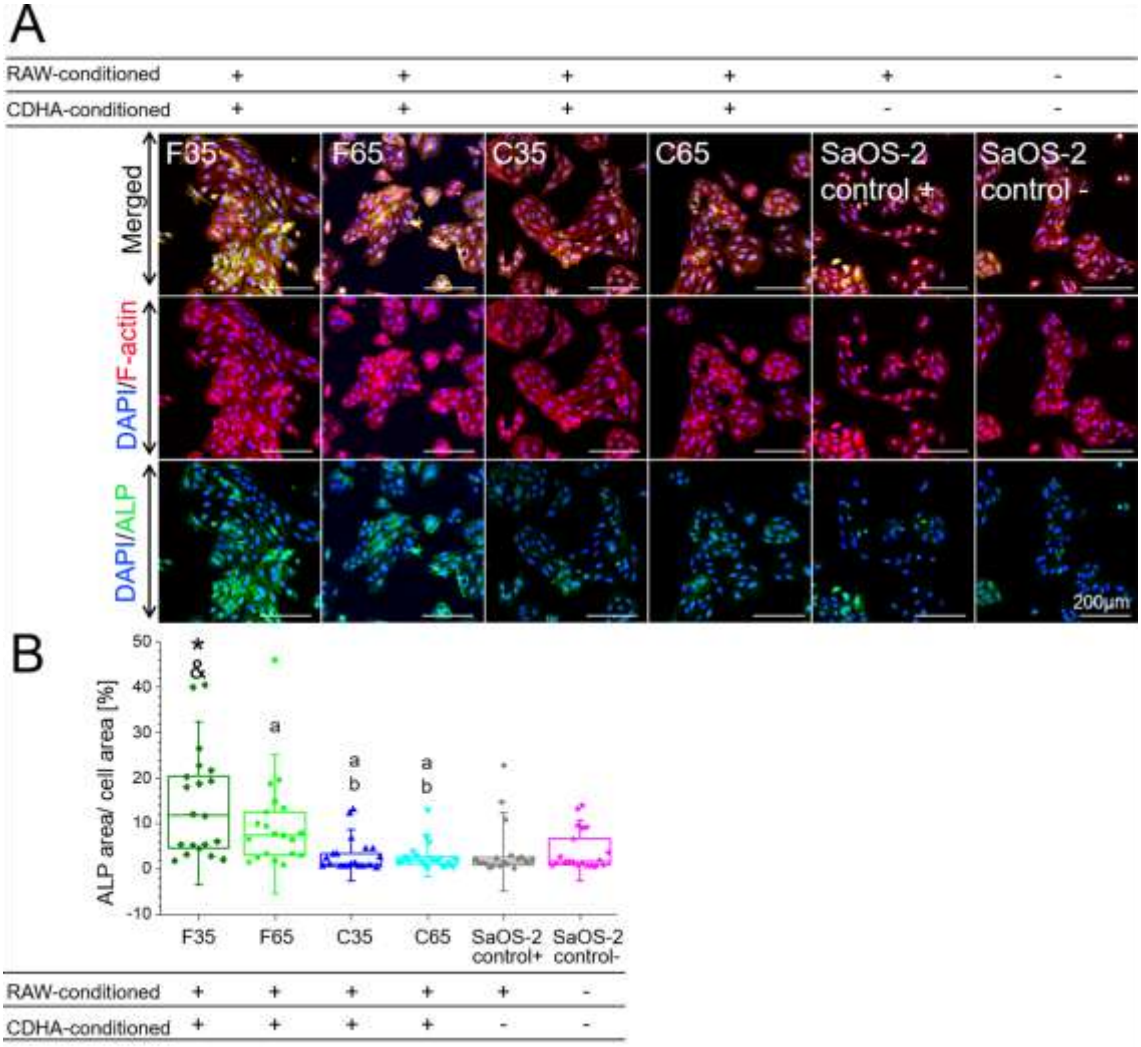

Figure 6. *Effect of CDHA- RAW cells conditioned medium on ALP expression of SaOS-2 cells.* **A)** *Representative confocal images of SaOS-2 morphology after 3 days of exposure to CDHA- RAW cells conditioned medium. Cells were stained for F-actin (red), nuclei (blue) and ALP (green). Scale bar in all images denotes 200 µm. The brightness and contrast of images was modified using Fiji/Image-J package.* **B)** *ALP area normalized to cell area after 3 days of culture. Symbols represent individual cells (n=20), the boxes represent 25th and 75th percentile, the middle line is the median and whiskers are standard deviation. * and & indicate statistically significant differences (P < 0.05) compared to the SaOS-2*

control+ and SaOS-2 control– groups, respectively. Statistically significant differences between substrates were indicated with letters (a, b) where a and b indicate statistically significant differences (P < 0.05) compared to F35 and F65 respectively. In both figures, "SaOS-2 control+" refers to osteoblastic cells stimulated with RAW cells conditioned medium (without CDHA substrate) whilst "SaOS-2 control-" refers to osteoblastic cells in their standard cell culture medium.

3.4. The effect of CDHA substrates on the response of RAW cells under inflammatory conditions

In order to evaluate the behaviour of immune cells on CDHA samples under inflammatory environment, macrophages were stimulated with 1 µg/ mL of LPS. Thereafter, morphological features of RAW cells as well as the expression of inflammatory, osteogenic and osteoclastogenic markers were analysed. Over the following sections, "control+" group refers to RAW cells cultured on TCPS and stimulated with LPS, whilst "control-" refers to RAW cells cultured on TCPS without any additional treatment.

3.4.1. RAW cells morphology

A combination of round-shaped cells with elongated cells was observed in all conditions (Figure 7). Moreover, the rounded cells showed more flattened morphology on CDHA with high L/P ratio. Noteworthy, image analysis revealed that LPS activated cells presented more spread morphology compared to control- group (Figure 7B). Even though, the spreading of macrophages on CDHA were less pronounced than cells cultured without any material and stimulated with LPS. The analysis of elongation ratio revealed higher elongation ratio for LPS stimulated cells.

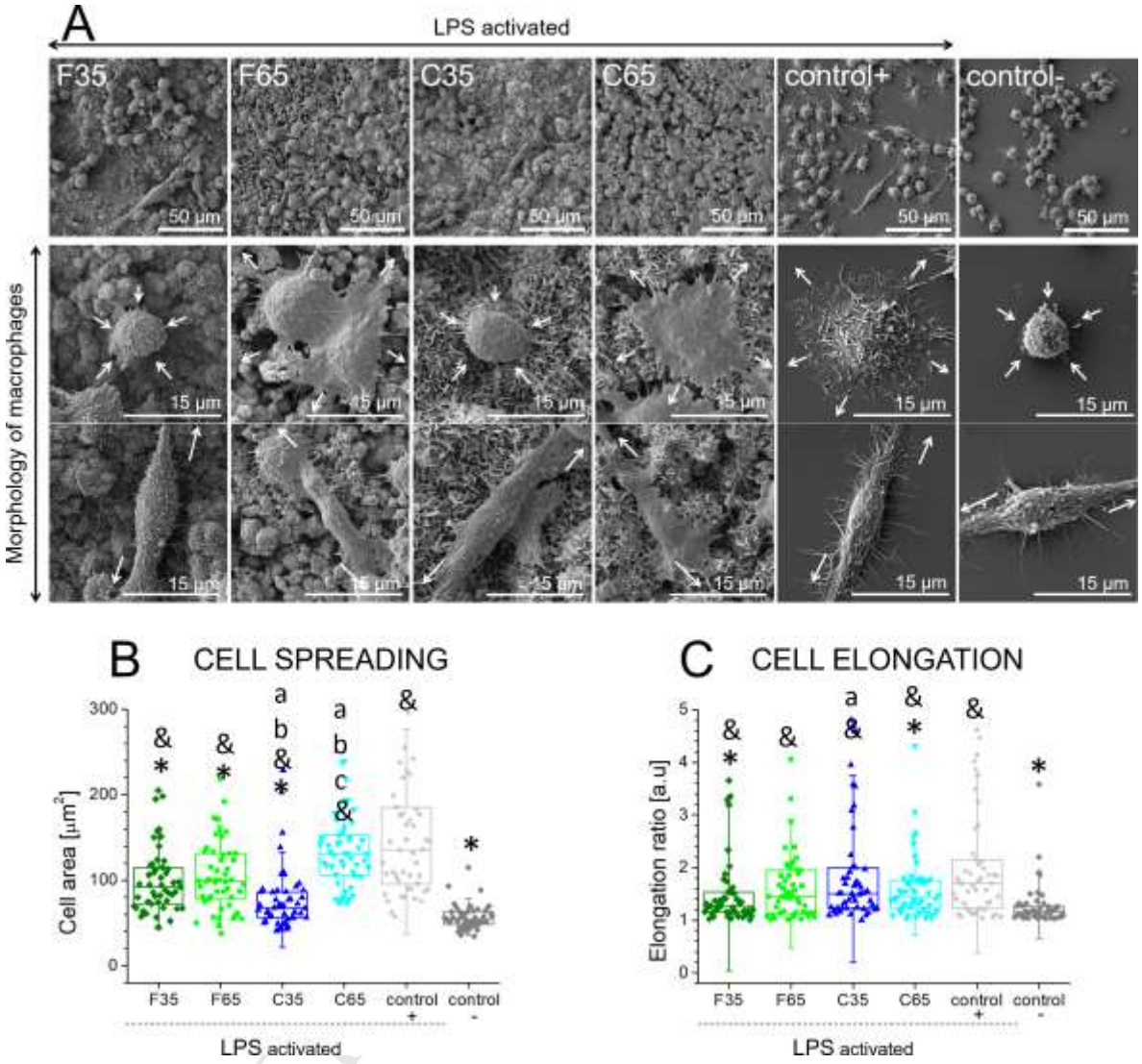

Figure 7. **A)** *Morphology of RAW cells observed by SEM on CDHA at 6 hours of post-stimulation. RAW cells cultured on glass coverslip were used as control, where "control+" represents LPS stimulated RAW cells and "control-" non-stimulated cells. Upper panel: general view. Middle and lower panel: detailed view of macrophages morphology. Both rounded and elongated-shape cells were found on CDHA substrates. RAW cells cultured on high L/P CDHA i.e. F65 and C65 showed more flattened morphologies compared to F35 and C35. The white arrows indicate a putative direction of cell spreading* **B)** *Cell spreading after LPS stimulation* **C)** *Cell elongation after LPS stimulation. In* **B** *and* **C**

*graphs, symbols represent individual cells (n=50), the boxes represent 25th and 75th percentile, the middle line is the median and whiskers are standard deviation. * and & Indicate statistically significant differences (P < 0.05) compared to the control+ group and control- group, respectively. Statistically significant differences between substrates were indicated with letters (a, b, c) where a, b and c indicate statistically significant differences (P < 0.05) compared to F35, F65 and C35, respectively.*

3.4.2. Inflammatory, osteogenic and osteoclastogenic gene expression of RAW cells

The inflammatory response of the macrophages cultured on CDHA samples under inflammatory environment is depicted in Figure 8A and D. Overall, biomimetic substrates showed antinflammatory features downregulating the expression of pro- inflammatory cytokines (IL-1β IL-6, TNFα) compared to control+ group. In general, the downregulation was more pronounced in the cells cultured on CDHA with low L/P ratio i.e. F35 and C35 compared to high L/P ratio equivalents. The evaluation of release of proinflammatory cytokines such as IL-6 and TNFαby ELISA (Figure 8D) confirmed similar trends to those observed by analysis of gene expression (Figure 8A). The expression of iNOS was slightly upregulated on C65 compared to control+.

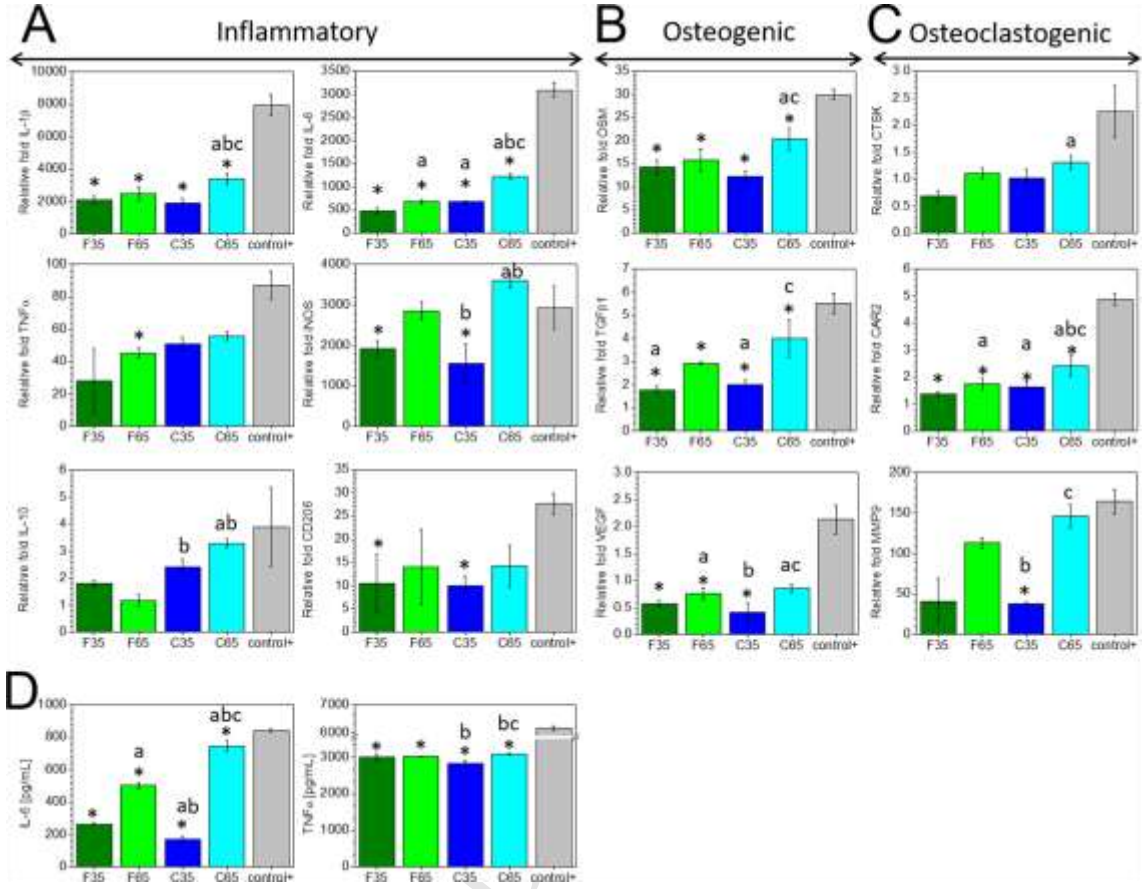

Figure 8. *Inflammatory, osteogenic and osteoclastogenic activity of RAW cells on CDHA substrates under inflammatory environment. Cells were collected at 6 hours post-stimulation with 1µg/ mL of LPS.* **A)** *Relative expressions of inflammation related genes; M1 markers: IL-1β, IL-6, TNFα, iNOS; M2 markers: IL-10, CD206.* **B)** *Relative expressions of osteogenesis related genes: OSM, TGFβ1, VEGF.* **C)** *Relative expressions of osteoclastogenesis related genes: CTSK, CAR2, MMP9. Gene expression results normalized with respect to housekeeping gene 18S using non-LPS stimulated RAW on TCPS as a calibrator sample.* **D)** *Release of inflammatory cytokines IL-6 and TNFα by RAW cells. Control+ represents LPS stimulated RAW cells cultured on TCPS. * Indicates statistically significant differences (P < 0.05) compared to the control+ group. Statistically significant differences between substrates are indicated with letters (a, b, c) where a, b and*

c indicates statistically significant differences ($P < 0.05$) compared to F35, F65 and C35 respectively.

Regarding the expression of antinflammatory IL-10 and CD206, the levels of both were slightly lower on biomimetic hydroxyapatite compared to control+. Needle like CDHA downregulated the expression of IL-10 to greater extent than plate- like substrate (Figure 8A).

Similar trends were observed for the osteogenic and osteoclastogenic activity of macrophages on the biomimetic CDHA substrates (Figure 8B and C). Overall, downregulation of osteogenetic (OSM, TGFβand VEGF) and osteoclastogenetic (CTSK, CAR2 and MMP) markers was observed on CDHA compared to control+, this trend being more pronounced for CDHA with low L/P ratio.

4. DISCUSSION

In the field of synthetic bone grafts, biomimetic calcium deficient hydroxyapatite presents interesting properties due to its similar composition and structure to the mineral phase of bone. Unlike for sintered calcium phosphate ceramics, the microstructure and porosity of this material can be easily tuned without modifying the chemical composition, covering a broad range of porosities and pore sizes and allowing to obtain nanostructured materials.[39] This offers a very versatile platform to study the effect of the textural properties of synthetic bone grafts on the interaction with cells and tissues. In this context it has been recently reported that the combined effect of nanostructure, poor crystallinity and favourable ionic microenvironment created in the proximity of the material confers CDHA superior osteoinductive properties in vivo. [40] However, information regarding the underlying mechanisms is scarce. Thus, the main motivation of this work was to study the

relevance of some textural properties of CDHA i.e. surface topography, SSA and porosity, on the immunomodulatory and osteoimmunomodulatory processes in vitro.

CDHA discs were obtained by cementitious reaction by the hydrolysis of αTCP.[34] Changing the particle size of the αTCP powder from fine (F) to coarse (C) shifted the size of the obtained crystals from the nano- to the micro-sized range, and the crystal morphology from needles to plates, respectively (Figure 1). The modification of the textural properties of CDHA resulted in significant changes of the SSA, surface roughness and stiffness (Table 2, Supplementary Figure 2 and Supplementary Figure 3). F substrates presented approximately two-fold SSA values than C substrates. Moreover, using two different L/P ratios i.e. low 0.35 mL/ g (F35 and C35) and high 0.65 ml/ g (F65 and C65) allowed tailoring the material porosity (Table 2).[34,35]Thus, chemically identical CDHA substrates were obtained, with distinct structural features. It is important to highlight that, unlike in the case of inert substrates, the variations in surface topography, SSA and porosity of CDHA are expected to affect the ionic exchange with the cell culture medium, which in turn may influence cell behaviour, as shown in previous studies.[37,41,42] Therefore, this creates a more complex scenario, since these indirect effects should be taken into consideration in addition to the direct effect of textural properties when evaluating immunomodulatory and osteoimmunomodulatory outcome of bioactive substrates.

In the present study we used RAW 246.7 cells as a model to study immune cell response to biomimetic hydroxyapatite with tailored characteristics. The evaluation of proliferation and morphology of macrophages are interesting tools towards discovering the severity of inflammation and immune cells' activation stage.[43] Our results revealed similar cell

adhesion on all biomimetic substrates, in agreement with previous findings (Figure 2A). [44] However, RAW cell proliferation was reduced on the CDHA substrates. This is in accordance with previous reports where biomimetic hydroxyapatite reduced the proliferation of various cell types, which was attributed to a coupled effect of spiky microstructure and altered ionic release/ uptake.[37,41,42] Similarly, Mestres et al. observed decreased cell number of RAW cells on CDHA at early days of cell culture being this scenario more pronounced for needle- like samples.[44] However, we did not observe this behaviour, which can be probably due to the use of smaller sample size, which reduced the extent of ionic fluctuations (Figure 4D).[45]

Macrophage morphology is generally associated with their polarization state. The round shape is usually related to pro- inflammatory M1 phenotype whereas M2 phenotype exhibit more elongated shapes.[46,47] In addition, M1 type is also accompanied with enhanced cell spreading after induction with LPS.[48] Nonetheless, it has to be considered that the macrophage morphological changes depend on the time of exposure to stimulating factors. [49,50] In addition, macrophages can be stimulated by the cytokines they produce and, with time, their functional pattern may shift in accordance. [51] Therefore, the evaluation of cytokine expression and secretion is a more precise indication of macrophage polarization than morphology.[52] Although we did not observe obvious changes in the elongation ratio of RAW cells (Figure 2B and D, Supplementary Figure 4), immune cells presented different spreading areas, depending of CDHA substrate (Figure 2B and C, Supplementary Figure 4). For instance, macrophages cultured on C65 presented enhanced spreading compared to the other biomimetic substrates and the control, suggesting a more inflammatory state. This agrees with findings by Mestres et al., who reported a higher

release of reactive oxygen species (ROS) for RAW cells cultured on plate- like substrates, suggesting a more inflammatory state compared to needle-like CDHA.[44]

Immediately after biomaterial implantation, immune cells are recruited and release pro-inflammatory molecules.[53] This process is particularly important due to the dual role of immune cells. Macrophages not only act as inflammatory mediators but also as wound and tissue healing regulators, determining further implant success or leading to chronic inflammation and graft rejection. Current strategies to control the foreign body response mostly focus on controlling inflammatory cytokines secretion. In this regard, modifications of the physicochemical features of biomaterials, including chemistry[24], roughness[54], stiffness[55] or geometry[56] have been reported to regulate macrophage activation. Interestingly, in our work higher values of pro-inflammatory cytokines IL-1β and IL-6 were observed on needle-like surfaces (F35), whereas TNFα was higher on plate-like surfaces. These results demonstrate that modifications at the nano- and micro-scale level influence differently macrophage activation, although in general the incubation with biomaterials fosters a pro-inflammatory status of immune cells as other authors previously described.[21,57,58] Our findings suggest that in our substrates there is no clear link between surface topography of CDHA and polarization of macrophages. One possible explanation might be bioactive nature of CaP substrates. For bioinert biomaterials the inflammatory molecule expression can be straightforwardly related to surface features in contrast to CDHA which ionic release/ uptake might interfere with the effect of surface topography on cytokine expression. Moreover, no correlation was found between the stiffness of the substrates and the morphology of immune cells. In fact, the Young's modulus of the substrates seem to be too high to be sensed by immune cells, which are usually activated by stiffness values in the range of kPa [29-31].

It is generally accepted that adherent macrophages produce a degradative microenvironment that accelerates biomaterial resorption. In our study, both needle-like and plate-like microstructures induced the generation of multinucleated cells (Supplementary Figure 6), with a morphology compatible with either osteoclastic cells or foreign body giant cells (FBGCs)- both known to have potential to dissolve hydroxyapatite crystals.[59]. Moreover, some degradation of the hydroxyapatite crystals was observed at the cell-substrate interface (Figure 4C), contrary to what happened in the substrates incubated with cell culture medium in absence of the macrophages, this suggesting a cell-mediated degradation. This agrees with our previous findings where prolonged exposure to cell culture medium did not affect the surface morphology of plate-like CDHA. [60] Higher levels of CAR2 and MMP9 were found when the cells were in contact with C substrates compared to their F counterparts with the same L/P ratio (C35 vs F35 and C65 an F65), indicating that greater surface roughness may trigger some degradative activity.[60,61] Another sign of degradative behaviour was the higher ion concentration, especially calcium, in the cell culture media in presence of macrophages compared to the cell-free substrates (Figure 4D). In fact, the release of these ions into the medium can be associated to the dissolution of CDHA by the activity of immune cells, which counteracts the ionic exchange produced by the material itself, similarly to what was found in a previous study.[60] As previously reported, the immersion of biomimetic hydroxyapatite in cell culture medium resulted in a decrease of the calcium concentration and a slight increase of phosphate.[37] This ionic fluctuations are caused by the uptake of calcium by the substrate due to the calcium deficient nature of biomimetic apatite, and the replacement of phosphate in the CDHA structure by other ions present in cell culture medium, mainly carbonate.[62] Interestingly, the higher the porosity and the SSA of the substrate, the higher were the ionic

fluctuations, being F65 the more reactive material. In presence of immune cells, an increase in Ca^{2+} concentration was observed for all substrates suggesting the cell- induced material degradation. However, is must be kept in mind that the differentiation of macrophages into fully functional osteoclasts[63] can be only achieved by additional stimulation with RANKL, OPG and M-CSF molecules.[64] Moreover, since the osteoclasts share many morphological similarities with FBGCs, it cannot be unambiguously claimed that CDHA stimulated osteoclastic differentiation of macrophages. However, it can be stated that the activity of RAW cells induced the degradation of CDHA surfaces.

The activation of immune cells and thus the simultaneous release of inflammatory molecules such as TNFα, TGFβ, INFγ and IL-17[12] or osteogenic factors like OSM, TGFβ1 and VEGF can also effectively stimulate osteoblastic differentiation. For instance, OSM, which is a pro-inflammatory cytokine of the IL-6 family secreted by M1 macrophages, was reported to promote osteoblastic differentiation and matrix mineralization[10], whereas VEGF, an anti-inflammatory cytokine produced by M2 macrophages, was recognised to be an osteogenic and angiogenic inducer.[14] In contrast, TGFβ1 exhibits a dual function; it can either stimulate osteogenesis[65] or lead to pathological fibrosis when its expression is prolonged.[66] Interestingly, in our study macrophages cultured on plate-like CDHA surfaces showed higher values of these gene markers compared to needle-like CDHA. On another hand, our results revealed an additional effect of substrate porosity on the secretion of osteogenic molecules by macrophages; the expression of all three genes was smaller in the samples with lower L/P ratio, i.e. low porosity, compared to their high L/P ratio, i.e. high porosity, equivalents (Figure 4A). In agreement with these results, Xiao et al. showed that that ceramic scaffolds with higher porosity led to increased expression of platelet- endothelial cell adhesion molecule (PECAM-1) and VEGF.[66]

To evaluate the influence of osteogenic factors and inflammatory molecules released by immune cells on osteoblastic differentiation, we cultured SaOS-2 cells with extracts from RAW cells cultured alone (control samples) or on the different CDHA substrates (Figure 5). Surprisingly, little impact of the extracts from RAW cells on the osteogenic gene expression of SaOS-2 was observed in the control samples. Although this might seem to contradict previous findings regarding the promotion of osteogenic differentiation of bone marrow MSCs by RAW cells extracts [16], it has to be considered that in the present study osteoblastic SaOS-2 cells were used instead of MSCs. Hence, the already differentiated osteoblast might be less sensitive to the effects of the microenvironment.[37] Although the expression of osteogenic molecules (OSM, TGFβ1 and VEFG) by RAW cells was generally lower for nanostructured needle- like substrates (Figure 4A), our results consistently showed that the immunoenvironment created by these CDHA materials stimulated to greater extent the expression of osteogenic- related genes as well as protein secretion in osteoblastic cells (Figure 5A, 5B and 6). This suggests the involvement of other osteogenic factors and inflammatory molecules, as previously observed in work of Chen et al.[21] Interestingly, macrophages cultured on needle-like surfaces overexpressed IL-1βand IL-6 cytokines, which might be responsible for enhanced osteogenesis of SaOS-2 after exposure to RAW and needle-like CDHA immunoenvironment. In fact, both cytokines have been reported to promote osteogenesis.[67,68,69] On the contrary, plate-like structures did not stimulate osteoblast differentiation probably due to the inhibitory effects of TNF-αsecreted by macrophages.[70,71] However, we cannot overlook the fact that the different substrates provoked different ionic fluctuations in the cell culture medium (Figure 4D). Both calcium and phosphate, either separately or simultaneously, are known to affect the osteogenic commitment of bone forming cells.[72–74] Therefore, the specific response of SaOS-2 cells

shouldn't be interpreted considering only the cytokines released in the supernatant by the macrophages. The changes in composition of the cell culture medium induced by the different substrates may also play a role, adding further complexity to the system and determining cell fate. However, we previously did not observe osteogenic differentiation of bone forming cells after exposure to CaPs modified cell culture medium[37], which suggests that the osteogenic differentiation is a result of the simultaneous effect of the microenvironment created by the substrate and the release of inflammatory molecules by macrophages, as observed by Chen et al.[16]

Finally, the effect of the physiochemical properties of CDHA on the anti-inflammatory capacity of RAW cells was also evaluated through the activation of the cells with LPS.[8] The activation of the immune cells was confirmed through visualisation of iNOS (Supplementary Figure 7), a common M1 phenotype reactive oxygen intermediate.[5] In general, the activation of immune cells led to different morphological (Figure 7, Supplementary Figure 8) and gene expression (Figure 8) responses to CDHA. This agrees with previous findings of Chen et al., who reported different behaviour of RAW cells cultured under standard and inflammatory conditions with mesoporous silica nanospheres.[8] The LPS stimulation led to more spread morphologies and elongation ratios compared to non- stimulated cells. Interestingly, high L/P ratio CDHA led to larger spreading areas compared to the equivalent substrates with low L/P ratio, suggesting that higher porosity stimulates the inflammation state to a greater extent. No clear effect of the needle- or plate-like microstructure was found. The results of inflammatory gene expression (Figure 8A) and cytokine release (Figure 8D) confirmed this trend. Interestingly, the incubation of macrophages with CDHA either under standard or inflammatory conditions led to different trends in terms of inflammatory gene expression

(Figures 3 and 8), which agrees with previous findings, where environment-depending response of macrophages to biomaterial was reported.[8] All the CDHA samples produced a reduction on the expression of inflammatory genes compared to the control after LPS induction, but the effect was more marked for the low L/P, this is, the less porous samples. The difference between F and C substrates, i.e. the effect of microstructure, was relevant only for the high L/P values, the F substrates showing lower expression of inflammation related genes. It has been observed previously that porous implants seem to modulate bone healing by inducing a shift in local macrophage phenotype into M1 phenotype, which in turn contribute to better vascularization an finally better integration of the implant.[27] On the other hand, topography may also play a role on the anti-inflammatory effects of CDHA, since needle-like structures reduced the expression of pro-inflammatory genes compared to plate-like structures, in agreement with a previous study.[44]

Activated macrophages cultured on CDHA expressed higher amounts of osteogenic and osteoclastogenic genes compared to non-activated macrophages, although the levels were lower than those of the control. Overall, our results suggest a predominant role of substrate porosity under inflammatory environment; the incubation of macrophages with CDHA with high L/P led to higher pro-inflammatory signalling compared to low L/P equivalents.

To further understand the effect of inflammatory conditions on the osteoimminomodulation process, SaOS-2 cells were incubated with CDHA-F- RAW conditioned medium in inflammatory conditions (Supplementary Figure 9), this is, after LPS-induction of RAW cells. Needle-like CDHA substrates were chosen because in standard conditions they created the more favourable osteogenic environment (Figure 5 and 6). However, contrary

to what happened in standard conditions, under inflammatory conditions the incubation of SaOS-2 cells with CDHA F-RAW conditioned medium did not promote the expression of osteogenic markers or the ALP production (Supplementary Figure 9). We hypothesize that this may be attributed to different cytokine and other inflammatory molecules release pattern from LPS-activated macrophages.[9]

Overall, the present work sheds light on the effect of structural differences of chemically identical calcium phosphate substrates on stimulating immunomodulatory, osteoimmunomodulatory and antinflammatory functions. The modification of surface topography and porosities of substrate will be an interesting tool for designing CaPs that trigger specific cellular responses of bone tissue.

5. CONCLUSIONS

The results obtained in this study demonstrated that the immune responses of macrophages can be modulated through distinct physicochemical properties of CDHA. Surface topography of CDHA plays an important role in stimulating the production of pro-inflammatory cytokines by macrophages, which in turn regulates osteogenic or degradative processes. Moreover, the results showed that nanostructured needle-like structures induce osteogenic activities of bone forming cells while porosity positively regulates the intensity of inflammation in CDHA substrates. Overall, our findings suggest that the favourable osteoimmune milieu for bone regeneration is not only related to the inflammatory cytokines released from activated immune cells, but also depends on the intrinsic microenvironment created by CDHA bioactivity.

As a proof of concept, the study was performed using well-characterized macrophage and osteoblast cell lines, RAW264.7 and SaOS-2 cells respectively, to understand whether the

cytokines generated by macrophages stimulated by the intrinsic microenvironment and the physicochemical properties of CDHA may influence the differentiation of osteoblasts. Considering the limitations of the use of cells lines, further studies using primary cells obtained from the same specie should be performed.

Acknowledgments

The authors acknowledge the Spanish Government for financial support through MAT2015-65601-R project, co-funded by the EU through European Regional Development Funds, and FPI scholarship of JMS. They also thank the Generalitat the Catalunya for funding through project 2017SGR-1165. MPG acknowledges the ICREA Academia award by the Generalitat de Catalunya.

AUTHOR INFORMATION

Corresponding authors:

E-mail: maria.pau.ginebra@upc.edu Tel: +34 93 401 77 06, Biomaterials, Biomechanics and Tissue Engineering Group, Department of Materials Science and Metallurgical Engineering, Universitat Politècnica de Catalunya (UPC), Av. Eduard Maristany 16, 08019 Barcelona, Spain

E-mail: yin.xiao@qut.edu.au. Tel: +61 7 31386240, Institute of Health and Biomedical Innovation, Queensland University of Technology, Brisbane, 60 Musk Ave, Kelvin Grove, Brisbane, Queensland 4059, Australia.

DATA AVAILABILITY

The raw/processed data required to reproduce these findings cannot be shared at this time as the data also forms part of an ongoing study.

References

[1] *Z. Chen, T. Klein, R.Z. Murray, R. Crawford, J. Chang, C. Wu, Y. Xiao, Osteoimmunomodulation for the development of advanced bone biomaterials, Mater. Today. 19 (2016) 304–321. doi:10.1016/j.mattod.2015.11.004.*

[2] *N. Mokarram, R. V Bellamkonda, A Perspective on Immunomodulation and Tissue Repair, Ann. Biomed. Eng. 42 (2014) 338–351. doi:10.1007/s10439-013-0941-0.*

[3] *X.Q. Wu, Y. Dai, Y. Yang, C. Huang, X.M. Meng, B.M. Wu, J. Li, Emerging role of microRNAs in regulating macrophage activation and polarization in immune response and inflammation, Immunology. 148 (2016) 237–248. doi:10.1111/imm.12608.*

[4] *D.Y.S. Vogel, J.E. Glim, A.W.D. Stavenuiter, M. Breur, P. Heijnen, S. Amor, C.D. Dijkstra, R.H.J. Beelen, Human macrophage polarization in vitro: Maturation and activation methods compared, Immunobiology. 219 (2014) 695–703. doi:10.1016/j.imbio.2014.05.002.*

[5] *U. Juhas, M. Ryba-Stanisławowska, P. Szargiej, J. Myśliwska, Different pathways of macrophage activation and polarization, Postepy Hig. Med. Dosw. 69 (2015) 496–502. doi:10.5604/17322693.1150133.*

[6] *Z. Chen, A. Bachhuka, F. Wei, X. Wang, G. Liu, K. Vasilev, Y. Xiao, Nanotopography-based strategy for the precise manipulation of osteoimmunomodulation in bone regeneration, Nanoscale. 9 (2017) 18129–18152. doi:10.1039/C7NR05913B.*

[7] *M.N. Michalski, L.K. McCauley, Macrophages and skeletal health, Pharmacol.*

Ther. 174 (2017) 43–54. doi:10.1016/j.pharmthera.2017.02.017.

[8] S. Han, Z. Chen, P. Han, Q. Hu, Y. Xiao, Activation of Macrophages by Lipopolysaccharide for Assessing the Immunomodulatory Property of Biomaterials, Tissue Eng. Part A. 23 (2017) 1100–1109. doi:10.1089/ten.tea.2016.0501.

[9] A. Mantovani, S.K. Biswas, M.R. Galdiero, A. Sica, M. Locati, Macrophage plasticity and polarization in tissue repair and remodelling, J. Pathol. 229 (2013) 176–185. doi:10.1002/path.4133.

[10] P. Guihard, Y. Danger, B. Brounais, E. David, R. Brion, J. Delecrin, C.D. Richards, S. Chevalier, F. Rédini, D. Heymann, H. Gascan, F. Blanchard, Induction of osteogenesis in mesenchymal stem cells by activated monocytes/macrophages depends on oncostatin M signaling, Stem Cells. 30 (2012) 762–772. doi:10.1002/stem.1040.

[11] J. Ding, O. Ghali, P. Lencel, O. Broux, C. Chauveau, J.C. Devedjian, P. Hardouin, D. Magne, TNF-α and IL-1β inhibit RUNX2 and collagen expression but increase alkaline phosphatase activity and mineralization in human mesenchymal stem cells, Life Sci. 84 (2009) 499–504. doi:10.1016/j.lfs.2009.01.013.

[12] L. Rifas, T-cell cytokine induction of BMP-2 regulates human mesenchymal stromal cell differentiation and mineralization, J. Cell. Biochem. 98 (2006) 706–714. doi:10.1002/jcb.20933.

[13] C.M. Champagne, J. Takebe, S. Offenbacher, L.F. Cooper, Macrophage cell lines produce osteoinductive signals that include bone morphogenetic protein-2, Bone. 30 (2002) 26–31. doi:10.1016/S8756-3282(01)00638-X.

[14] D.O. Freytes, J.W. Kang, I. Marcos-Campos, G. Vunjak-Novakovic, Macrophages modulate the viability and growth of human mesenchymal stem cells, J. Cell.

Biochem. 114 (2013) 220–229. doi:10.1002/jcb.24357.

[15] Z. Chen, X. Mao, L. Tan, T. Friis, C. Wu, R. Crawford, Y. Xiao, Osteoimmunomodulatory properties of magnesium scaffolds coated with β-tricalcium phosphate, Biomaterials. 35 (2014) 8553–8565. doi:10.1016/j.biomaterials.2014.06.038.

[16] Z. Chen, C. Wu, W. Gu, T. Klein, R. Crawford, Y. Xiao, Osteogenic differentiation of bone marrow MSCs by β-tricalcium phosphate stimulating macrophages via BMP2 signalling pathway., Biomaterials. 35 (2014) 1507–18. doi:10.1016/j.biomaterials.2013.11.014.

[17] S. Chen, J.A. Jones, Y. Xu, H.Y. Low, J.M. Anderson, K.W. Leong, Characterization of topographical effects on macrophage behavior in a foreign body response model, Biomaterials. 31 (2010) 3479–3491. doi:10.1016/j.biomaterials.2010.01.074.

[18] M.L. Godek, J.A. Sampson, N.L. Duchsherer, Q. McElwee, D.W. Grainger, Rho GTPase protein expression and activation in murine monocytes/macrophages are not modulated by model biomaterial surfaces in serum-containing in vitro cultures, J. Biomater. Sci. Polym. Ed. 17 (2006) 1141–1158. doi:10.1163/156856206778530731.

[19] P.C.S. Bota, A.M.B. Collie, P. Puolakkainen, R.B. Vernon, E.H. Sage, B.D. Ratner, P.S. Stayton, Biomaterial topography alters healing in vivo and monocyte/macrophage activation in vitro, J. Biomed. Mater. Res. - Part A. 95 A (2010) 649–657. doi:10.1002/jbm.a.32893.

[20] B. Wójciak-Stothard, A. Curtis, W. Monaghan, K. Macdonald, C. Wilkinson, Guidance and activation of murine macrophages by nanometric scale topography, Exp. Cell Res. 223 (1996) 426–435. doi:10.1006/excr.1996.0098.

[21] *Z. Chen, A. Bachhuka, S. Han, F. Wei, S. Lu, R.M. Visalakshan, K. Vasilev, Y. Xiao, Tuning Chemistry and Topography of Nanoengineered Surfaces to Manipulate Immune Response for Bone Regeneration Applications, ACS Nano. 11 (2017) 4494–4506. doi:10.1021/acsnano.6b07808.*

[22] *Y. Arima, H. Iwata, Effect of wettability and surface functional groups on protein adsorption and cell adhesion using well-defined mixed self-assembled monolayers, Biomaterials. 28 (2007) 3074–3082. doi:10.1016/j.biomaterials.2007.03.013.*

[23] *N. Faucheux, R. Schweiss, K. Lützow, C. Werner, T. Groth, Self-assembled monolayers with different terminating groups as model substrates for cell adhesion studies, Biomaterials. 25 (2004) 2721–2730. doi:10.1016/j.biomaterials.2003.09.069.*

[24] *R.J. Schutte, A. Parisi-Amon, W.M. Reichert, Cytokine profiling using monocytes/macrophages cultured on common biomaterials with a range of surface chemistries, J. Biomed. Mater. Res. - Part A. 88 (2009) 128–139. doi:10.1002/jbm.a.31863.*

[25] *J.E. McBane, L.A. Matheson, S. Sharifpoor, J.P. Santerre, R.S. Labow, Effect of polyurethane chemistry and protein coating on monocyte differentiation towards a wound healing phenotype macrophage, Biomaterials. 30 (2009) 5497–5504. doi:10.1016/j.biomaterials.2009.07.010.*

[26] *V. Ballotta, A. Driessen-Mol, C.V.C. Bouten, F.P.T. Baaijens, Strain-dependent modulation of macrophage polarization within scaffolds, Biomaterials. 35 (2014) 4919–4928. doi:10.1016/j.biomaterials.2014.03.002.*

[27] *E.M. Sussman, M.C. Halpin, J. Muster, R.T. Moon, B.D. Ratner, Porous implants modulate healing and induce shifts in local macrophage polarization in the foreign*

body reaction, Ann. Biomed. Eng. 42 (2014) 1508–1516. doi:10.1007/s10439-013-0933-0.

[28] D. Bezuidenhout, N. Davies, P. Zilla, Effect of well defined dodecahedral porosity on inflammation and angiogenesis., ASAIO J. 48 (2002) 465–71. doi:10.1097/01.MAT.0000026345.66193.59.

[29] K.M. Adlerz, H. Aranda-Espinoza, H.N. Hayenga, Substrate elasticity regulates the behavior of human monocyte-derived macrophages, Eur. Biophys. J. 45 (2016) 301–309. doi:10.1007/s00249-015-1096-8.

[30] X.T. He, R.X. Wu, X.Y. Xu, J. Wang, Y. Yin, F.M. Chen, Macrophage involvement affects matrix stiffness-related influences on cell osteogenesis under three-dimensional culture conditions, Acta Biomater. 71 (2018) 132–147. doi:10.1016/j.actbio.2018.02.015.

[31] M. Friedemann, L. Kalbitzer, S. Franz, S. Moeller, M. Schnabelrauch, J.C. Simon, T. Pompe, K. Franke, Instructing Human Macrophage Polarization by Stiffness and Glycosaminoglycan Functionalization in 3D Collagen Networks, Adv. Healthc. Mater. 6 (2017). doi:10.1002/adhm.201600967.

[32] Z. Chen, J. Yuen, R. Crawford, J. Chang, C. Wu, Y. Xiao, The effect of osteoimmunomodulation on the osteogenic effects of cobalt incorporated β-tricalcium phosphate, Biomaterials. 61 (2015) 126–138. doi:10.1016/j.biomaterials.2015.04.044.

[33] Z. Chen, S. Ni, S. Han, R. Crawford, S. Lu, F. Wei, J. Chang, C. Wu, Y. Xiao, Nanoporous microstructures mediate osteogenesis by modulating the osteo-immune response of macrophages, Nanoscale. 9 (2017) 706–718. doi:10.1039/C6NR06421C.

[34] M.P. Ginebra, E. Fernández, E. a. P. a De Maeyer, R.M.H.M. Verbeeck, M.G.G.

Boltong, J. Ginebra, F.C. Driessens, J. a. a Planell, E. Fernandez, E. a. P. a De Maeyer, R.M.H.M. Verbeeck, M.G.G. Boltong, J. Ginebra, F.C. Driessens, J. a. a Planell, Setting Reaction and Hardening of an Apatitic Calcium Phosphate Cement, J. Dent. Res. 76 (1997) 905–912. doi:10.1177/00220345970760041201.

[35] M. Espanol, R. a Perez, E.B. Montufar, C. Marichal, a Sacco, M.P. Ginebra, Intrinsic porosity of calcium phosphate cements and its significance for drug delivery and tissue engineering applications., Acta Biomater. 5 (2009) 2752–62. doi:10.1016/j.actbio.2009.03.011.

[36] K.J. Livak, T.D. Schmittgen, Analysis of relative gene expression data using real-time quantitative PCR and the 2-ΔΔCT method, Methods. 25 (2001) 402–408. doi:10.1006/meth.2001.1262.

[37] J.-M. Sadowska, J. Guillem-Marti, E.B. Montufar, M. Espanol, M.-P. Ginebra, Biomimetic Versus Sintered Calcium Phosphates: The In Vitro Behavior of Osteoblasts and Mesenchymal Stem Cells, Tissue Eng. Part A. 23 (2017) 1297–1309. doi:10.1089/ten.tea.2016.0406.

[38] A. Diez-Escudero, M. Espanol, S. Beats, M.-P. Ginebra, In vitro degradation of calcium phosphates: Effect of multiscale porosity, textural properties and composition, Acta Biomater. 60 (2017) 81–92. doi:10.1016/j.actbio.2017.07.033.

[39] D. Pastorino, C. Canal, M.P. Ginebra, Multiple characterization study on porosity and pore structure of calcium phosphate cements, Acta Biomater. 28 (2015) 205–214. doi:10.1016/j.actbio.2015.09.017.

[40] A. Barba, A. Diez-Escudero, Y. Maazouz, K. Rappe, M. Espanol, E.B. Montufar, M. Bonany, J.M. Sadowska, J. Guillem-Marti, C. Öhman-Mägi, C. Persson, M.C. Manzanares, J. Franch, M.P. Ginebra, Osteoinduction by Foamed and 3D-Printed

Calcium Phosphate Scaffolds: Effect of Nanostructure and Pore Architecture, ACS Appl. Mater. Interfaces. 9 (2017) 41722–41736. doi:10.1021/acsami.7b14175.

[41] J. Gustavsson, M.P. Ginebra, J. Planell, E. Engel, Osteoblast-like cellular response to dynamic changes in the ionic extracellular environment produced by calcium-deficient hydroxyapatite., J. Mater. Sci. Mater. Med. 23 (2012) 2509–20. doi:10.1007/s10856-012-4705-4.

[42] E. Engel, S. Del Valle, C. Aparicio, G. Altankov, L. Asin, J. a Planell, M.-P. Ginebra, Discerning the role of topography and ion exchange in cell response of bioactive tissue engineering scaffolds., Tissue Eng. Part A. 14 (2008) 1341–51. doi:10.1089/ten.tea.2007.0287.

[43] S.J. Jenkins, D. Ruckerl, P.C. Cook, L.H. Jones, F.D. Finkelman, N. van Rooijen, A.S. MacDonald, J.E. Allen, Local Macrophage Proliferation, Rather than Recruitment from the Blood, Is a Signature of TH2 Inflammation, Science (80-.). 332 (2011) 1284–1288. doi:10.1126/science.1204351.

[44] G. Mestres, M. Espanol, W. Xia, C. Persson, M.P. Ginebra, M.K. Ott, Inflammatory response to nano- And microstructured hydroxyapatite, PLoS One. 10 (2015) 1–20. doi:10.1371/journal.pone.0120381.

[45] J.-M. Sadowska, J. Guillem-Marti, M. Espanol, C. Stähli, N. Döbelin, M.-P. Ginebra, In vitro response of mesenchymal stem cells to biomimetic hydroxyapatite substrates: a new strategy to assess the effect of ion exchange, Acta Biomater. (2018). doi:10.1016/j.actbio.2018.06.025.

[46] R. Sridharan, A.R. Cameron, D.J. Kelly, C.J. Kearney, F.J. O'Brien, F.J.O. Brien, Biomaterial based modulation of macrophage polarization: A review and suggested design principles, Mater. Today. 18 (2015) 313–325.

doi:10.1016/j.mattod.2015.01.019.

[47] F.Y. McWhorter, T. Wang, P. Nguyen, T. Chung, W.F. Liu, Modulation of macrophage phenotype by cell shape, Proc. Natl. Acad. Sci. 110 (2013) 17253–17258. doi:10.1073/pnas.1308887110.

[48] A. Schmidt, E. Caron, A. Hall, Lipopolysaccharide-Induced Activation of 2-Integrin Function in Macrophages Requires Irak Kinase Activity, p38 Mitogen- Activated Protein Kinase, and the Rap1 GTPase, Mol. Cell. Biol. 21 (2001) 438–448. doi:10.1128/MCB.21.2.438-448.2001.

[49] C.A. Wells, T. Ravasi, G.J. Faulkner, P. Carninci, Y. Okazaki, Y. Hayashizaki, M. Sweet, B.J. Wainwright, D.A. Hume, Genetic control of the innate immune response., BMC Immunol. 4 (2003) 5. doi:10.1186/1471-2172-4-5.

[50] W. Shurety, A. Merino-Trigo, D. Brown, D.A. Hume, J.L. Stow, Localization and Post-Golgi Trafficking of Tumor Necrosis Factor-alpha in Macrophages, J. Interf. Cytokine Res. 20 (2000) 427–438. doi:10.1089/107999000312379.

[51] R.D. Stout, C. Jiang, B. Matta, I. Tietzel, S.K. Watkins, J. Suttles, Macrophages Sequentially Change Their Functional Phenotype in Response to Changes in Microenvironmental Influences, J. Immunol. 175 (2005) 342–349. doi:10.4049/jimmunol.175.1.342.

[52] F.O. Martinez, S. Gordon, M. Locati, A. Mantovani, Transcriptional Profiling of the Human Monocyte-to-Macrophage Differentiation and Polarization: New Molecules and Patterns of Gene Expression, J. Immunol. 177 (2006) 7303–7311. doi:10.4049/jimmunol.177.10.7303.

[53] M. Scatena, K. V. Eaton, M.F. Jackson, S.A. Lund, C.M. Giachelli, Macrophages: The Bad, the Ugly, and the Good in the Inflammatory Response to Biomaterials, in:

Immune Response to Implant. Mater. Devices, Springer International Publishing, Cham, 2017: pp. 37–62. doi:10.1007/978-3-319-45433-7_3.

[54] A.K. Refai, M. Textor, D.M. Brunette, J.D. Waterfield, Effect of titanium surface topography on macrophage activation and secretion of proinflammatory cytokines and chemokines, J. Biomed. Mater. Res. 70A (2004) 194–205. doi:10.1002/jbm.a.30075.

[55] S. Féréol, R. Fodil, B. Labat, S. Galiacy, V.M. Laurent, B. Louis, D. Isabey, E. Planus, Sensitivity of alveolar macrophages to substrate mechanical and adhesive properties, Cell Motil. Cytoskeleton. 63 (2006) 321–340. doi:10.1002/cm.20130.

[56] G. Voskerician, P.H. Gingras, J.M. Anderson, Macroporous condensed poly(tetrafluoroethylene). I. In vivo inflammatory response and healing characteristics, J. Biomed. Mater. Res. - Part A. 76 (2006) 234–242. doi:10.1002/jbm.a.30481.

[57] N.E. Paul, C. Skazik, M. Harwardt, M. Bartneck, B. Denecke, D. Klee, J. Salber, G. Zwadlo-Klarwasser, Topographical control of human macrophages by a regularly microstructured polyvinylidene fluoride surface, Biomaterials. 29 (2008) 4056–4064. doi:10.1016/j.biomaterials.2008.07.010.

[58] K.M. Hotchkiss, G.B. Reddy, S.L. Hyzy, Z. Schwartz, B.D. Boyan, R. Olivares-Navarrete, Titanium surface characteristics, including topography and wettability, alter macrophage activation, Acta Biomater. 31 (2016) 425–434. doi:10.1016/j.actbio.2015.12.003.

[59] B. Ten Harkel, T. Schoenmaker, D.I. Picavet, N.L. Davison, T.J. De Vries, V. Everts, The foreign body giant cell cannot resorb bone, but dissolves hydroxyapatite like osteoclasts, PLoS One. 10 (2015) 1–19. doi:10.1371/journal.pone.0139564.

[60] G. Ciapetti, G. Di Pompo, S. Avnet, D. Martini, A. Diez-Escudero, E.B. Montufar, M.-P. Ginebra, N. Baldini, Osteoclast differentiation from human blood precursors on biomimetic calcium-phosphate substrates, Acta Biomater. 50 (2017) 102–113. doi:10.1016/j.actbio.2016.12.013.

[61] J. Costa-Rodrigues, A. Fernandes, M.A. Lopes, M.H. Fernandes, Hydroxyapatite surface roughness: Complex modulation of the osteoclastogenesis of human precursor cells, Acta Biomater. 8 (2012) 1137–1145. doi:10.1016/j.actbio.2011.11.032.

[62] S. Cazalbou, C. Combes, D. Eichert, C. Rey, M.J. Glimcher, Poorly crystalline apatites: evolution and maturation in vitro and in vivo., J. Bone Miner. Metab. 22 (2004) 310–7. doi:10.1007/s00774-004-0488-0.

[63] B. ten Harkel, T. Schoenmaker, D.I. Picavet, N.L. Davison, T.J. de Vries, V. Everts, The Foreign Body Giant Cell Cannot Resorb Bone, But Dissolves Hydroxyapatite Like Osteoclasts, PLoS One. 10 (2015) e0139564. doi:10.1371/journal.pone.0139564.

[64] S.L. Teitelbaum, Bone resorption by osteoclasts, Science 289 (2000) 1504–1508. doi:10.1126/science.289.5484.1504.

[65] M. Mizuno, Y. Kuboki, TGF-βAccelerated the Osteogenic Differentiation of Bone Marrow Cells Induced by Collagen Matrix, Biochem. Biophys. Res. Commun. 211 (1995) 1091–1098. doi:10.1006/bbrc.1995.1923.

[66] Z. Chen, C. Wu, Y. Xiao, Convergence of Osteoimmunology and Immunomodulation for the Development and Assessment of Bone Biomaterials, in: Immune Response to Implant. Mater. Devices, Springer International Publishing, Cham, 2017: pp. 107–124. doi:10.1007/978-3-319-45433-7_6.

[67] *F.-H. Lin, J.B. Chang, M.H. McGuire, J.A. Yee, B.E. Brigman, Biphasic effects of interleukin-1β on osteoblast differentiation in vitro, J. Orthop. Res. (2010) n/a-n/a. doi:10.1002/jor.21099.*

[68] *J.E. Huh, S.Y. Lee, IL-6 is produced by adipose-derived stromal cells and promotes osteogenesis, Biochim. Biophys. Acta - Mol. Cell Res. 1833 (2013) 2608–2616. doi:10.1016/j.bbamcr.2013.06.025.*

[69] *T.J. Cho, J.A. Kim, C.Y. Chung, W.J. Yoo, L.C. Gerstenfeld, T.A. Einhorn, I.H. Choi, Expression and role of interleukin-6 in distraction osteogenesis, Calcif. Tissue Int. 80 (2007) 192–200. doi:10.1007/s00223-006-0240-y.*

[70] *L. Gilbert, X. He, P. Farmer, S. Boden, M. Kozlowski, J. Rubin, M.S. Nanes, Inhibition of Osteoblast Differentiation by Tumor Necrosis Factor-α, Endocrinology. 141 (2000) 3956–3964. doi:doi:10.1210/endo.141.11.7739.*

[71] *L. Zhao, J. Huang, H. Zhang, Y. Wang, L.E. Matesic, M. Takahata, H. Awad, D. Chen, L. Xing, Tumor necrosis factor inhibits mesenchymal stem cell differentiation into osteoblasts via the ubiquitin E3 ligase Wwp1, Stem Cells. 29 (2011) 1601–1610. doi:10.1002/stem.703.*

[72] *A. Barradas, H. Yuan, C. van Blitterswijk, P. Habibovic, Osteoinductive biomaterials: current knowledge of properties, experimental models and biological mechanisms, Eur. Cells Mater. 21 (2011) 407–429. doi:10.22203/eCM.v021a31.*

[73] *A.M.C. Barradas, H. Yuan, J. van der Stok, B. Le Quang, H. Fernandes, A. Chaterjea, M.C.H. Hogenes, K. Shultz, L.R. Donahue, C. van Blitterswijk, J. de Boer, The influence of genetic factors on the osteoinductive potential of calcium phosphate ceramics in mice., Biomaterials. 33 (2012) 5696–705. doi:10.1016/j.biomaterials.2012.04.021.*

[74] *H. Yuan, H. Fernandes, P. Habibovic, J. de Boer, A.M.C. Barradas, A. de Ruiter, W.R. Walsh, C.A. van Blitterswijk, J.D. de Bruijn, A.M. C Barradas, A. de Ruiter, W.R. Walsh, C.A. van Blitterswijk, J.D. de Bruijn. Osteoinductive ceramics as a synthetic alternative to autologous bone grafting., Proc. Natl. Acad. Sci. U. S. A. 107 (2010) 13614–9. doi:10.1073/pnas.1003600107.*

SUPPLEMENTARY DATA

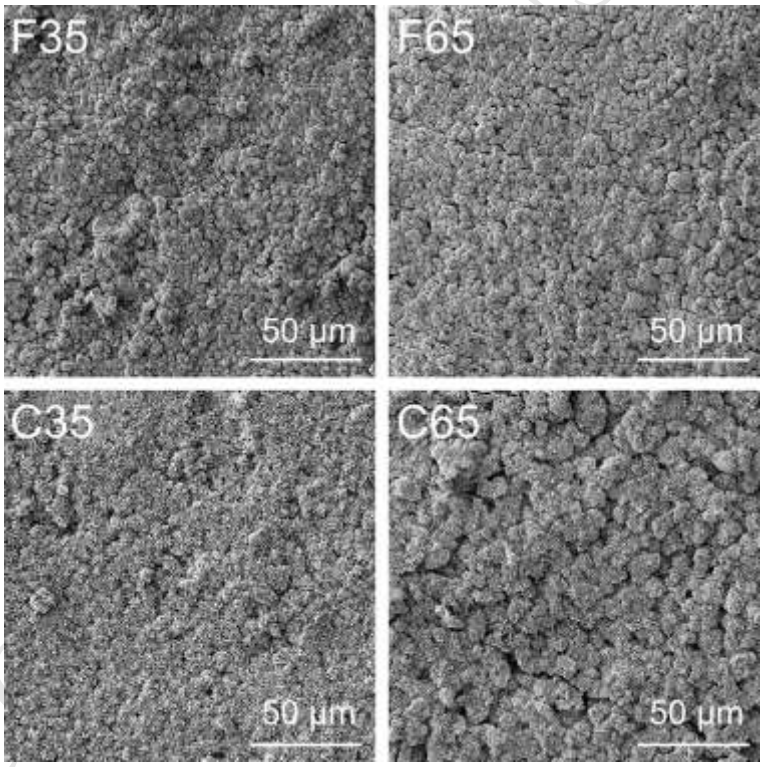

Supplementary Figure 1. *General view of the surface of the different CDHA substrates at low magnification.*

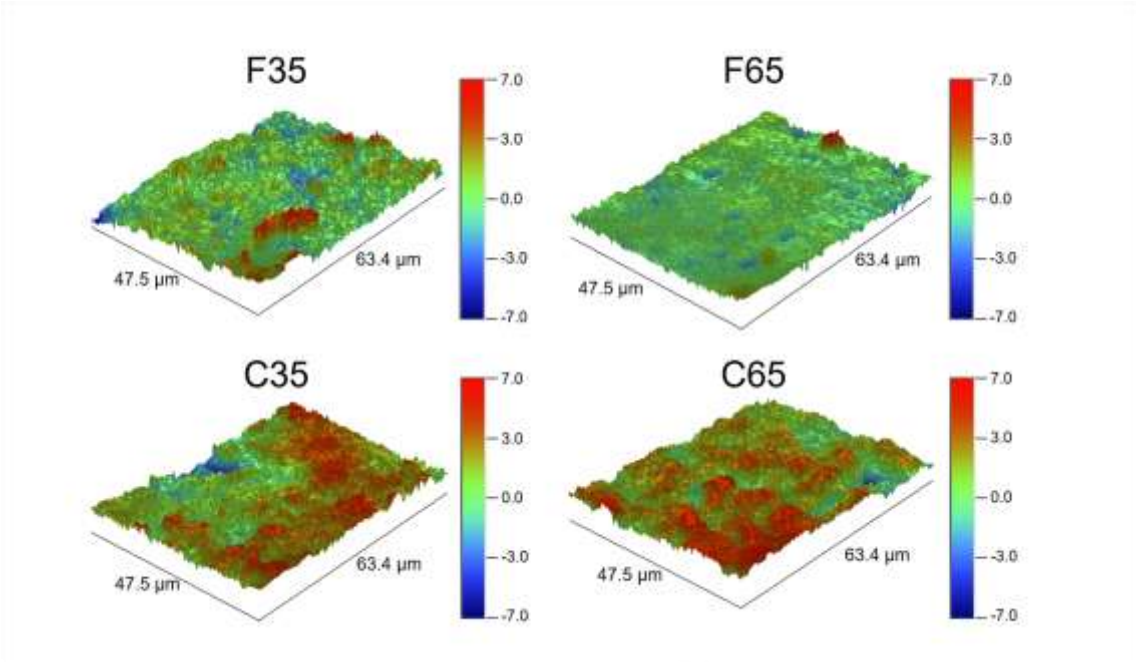

Supplementary Figure 2. *Optical interferometry images of surface topography of CDHA substrates.*

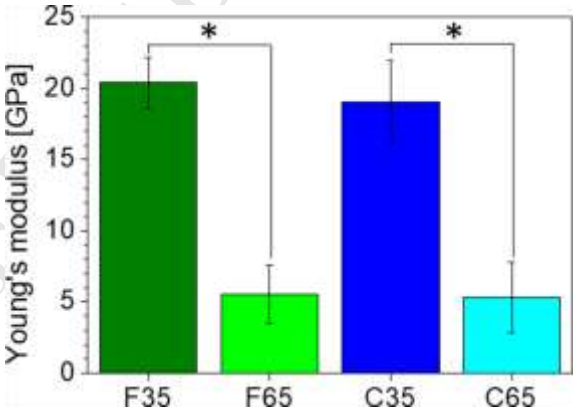

Supplementary Figure 3. *Young's modulus of the different CDHA substrates. * Indicates statistically significant differences (P < 0.05) between substrates. For mechanical testing, cylinders of 6 mm of diameter and 12 mm of height were prepared following the protocol described in section 2.1. Afterwards, the samples (n=10) were subjected to a compression test at a crosshead speed of 1 mm/ min in a Universal Testing Machine (Adamel Lhomargy DY 34). The Young's modulus was calculated from the stress-strain curve.*

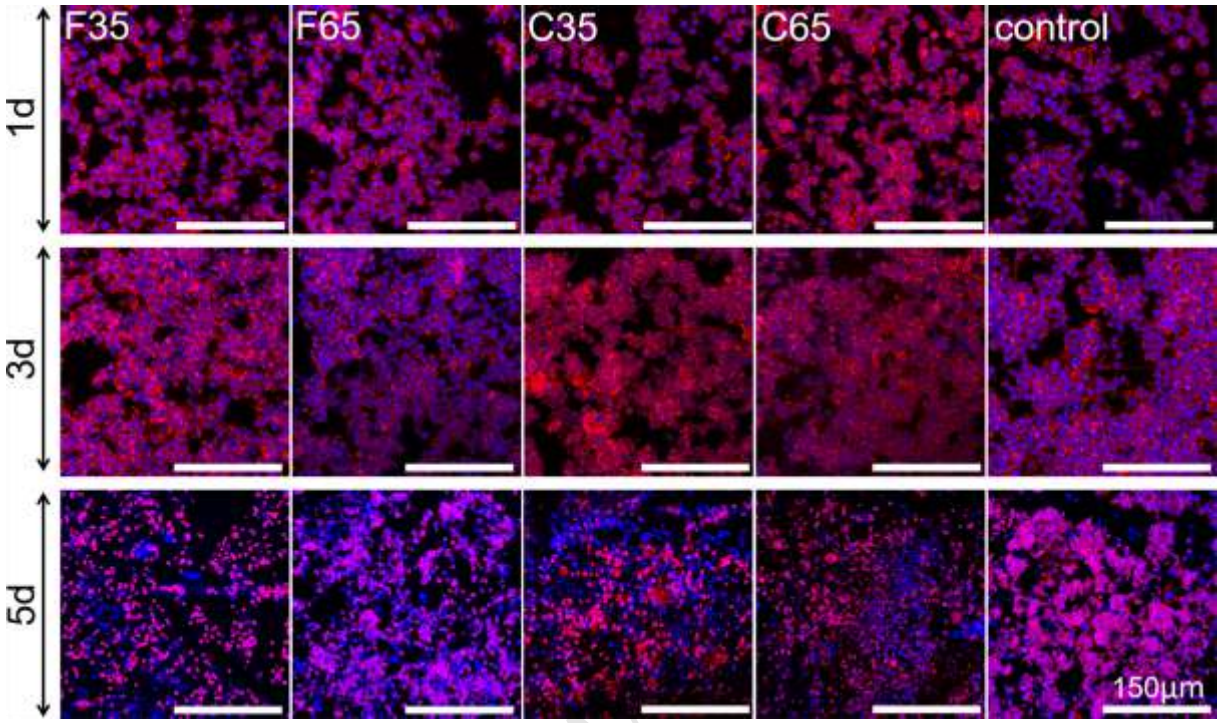

Supplementary Figure 4. *Representative confocal images of the morphology of RAW 264.7 cells on nano- and micro-structured biomimetic hydroxyapatite at 1,3 and 5 days of cell culture. Cells were stained for F-actin (red) and nuclei (blue). RAW 264.7 seeded on glass coverslip were used as a control group. Scale bar in all images denotes 150 µm. The brightness and contrast of images was modified using Fiji/Image-J package.*

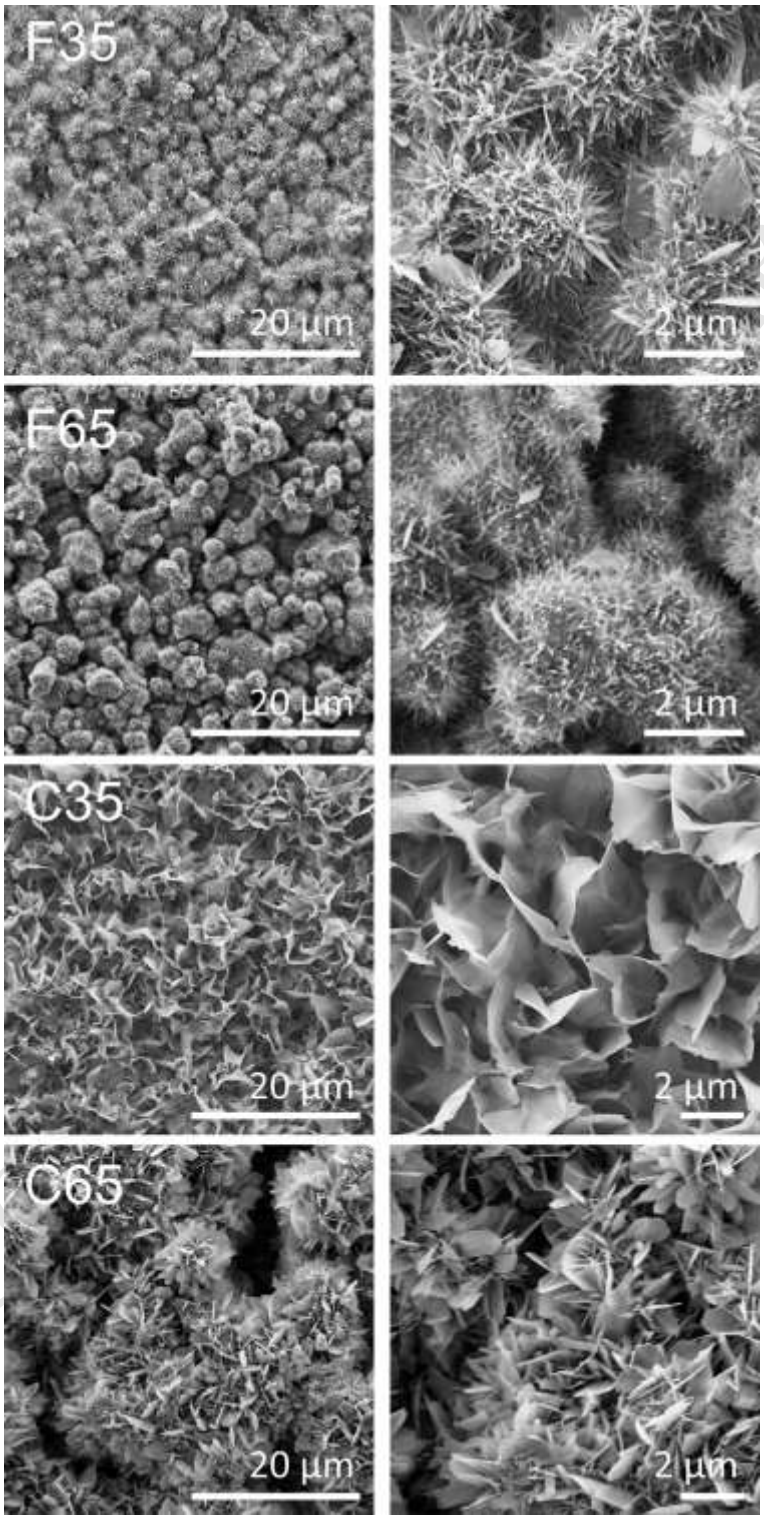

Supplementary Figure 5. *SEM images of the surface morphology of CDHA after 3 days incubation in cell culture medium in absence of cells.*

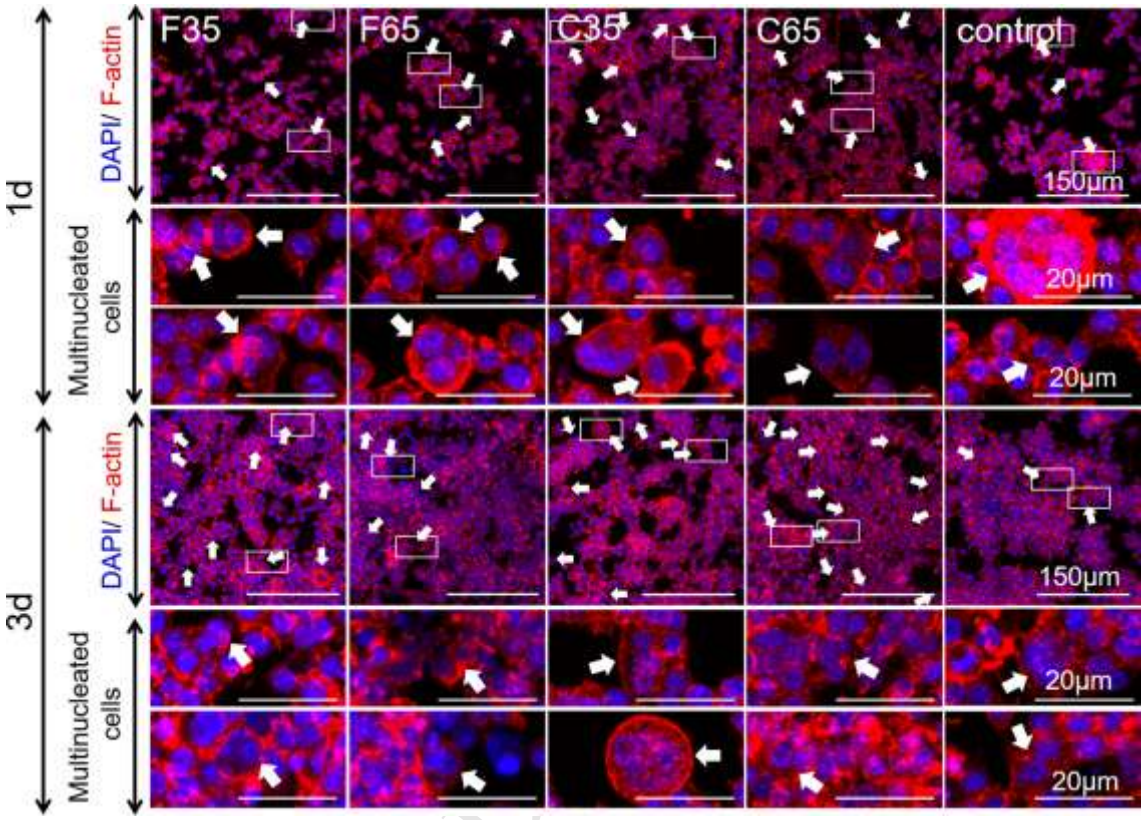

Supplementary Figure 6. *Numerous multinucleated cells (white arrows) were observed on nano- and microstructured hydroxyapatite at 1 and 3 days of cell culture. Cells were stained for F-actin (red) and nuclei (blue). RAW seeded on glass coverslip were used as a control group. The study revealed greater number of multinucleated cells on CDHA substrates compared to the control. Scale denotes 150 μm and for magnified images 20 μm. . The brightness and contrast of images was modified using Fiji/Image-J package.*

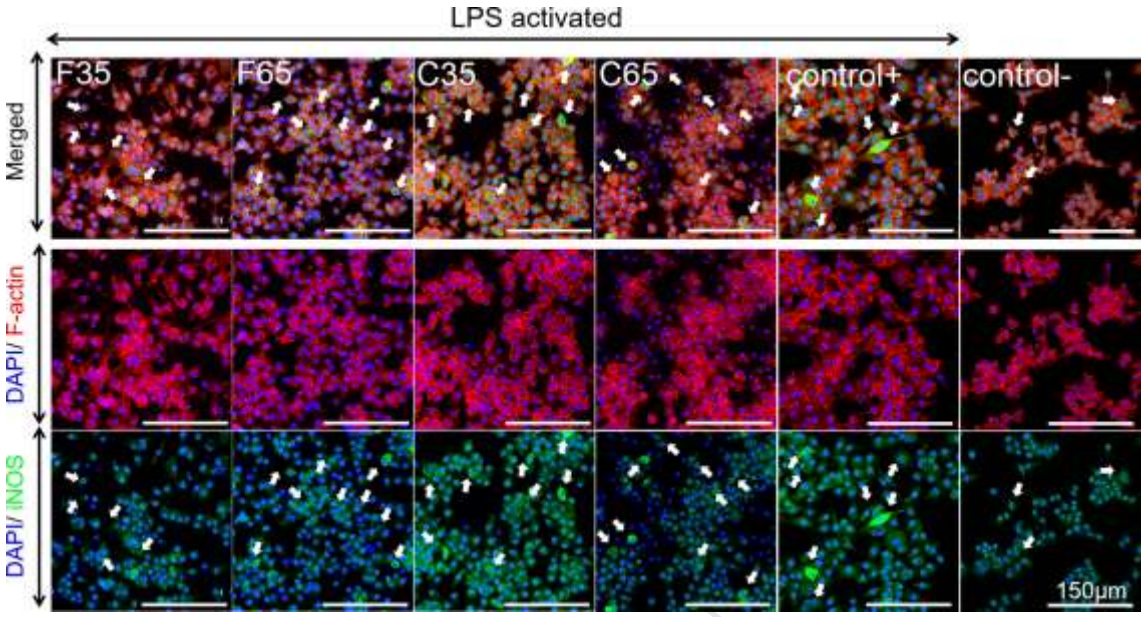

Supplementary Figure 7. *Presence of iNOS- positively stained cells (white arrows) on CDHA substrates 6 hours after LPS stimulation. Cells were stained for F-actin (red), nuclei (blue) and iNOS (green). RAW cells seeded on glass coverslip were used as a control group. Control+ represents cells with LPS stimulation whilist control- cells without LPS stimulation. The iNOS staining of RAW cells confirmed successfully induced inflammatory environment on CDHA and control+. Scale denotes 150 µm. The brightness and contrast of images was modified using Fiji/Image-J package.*

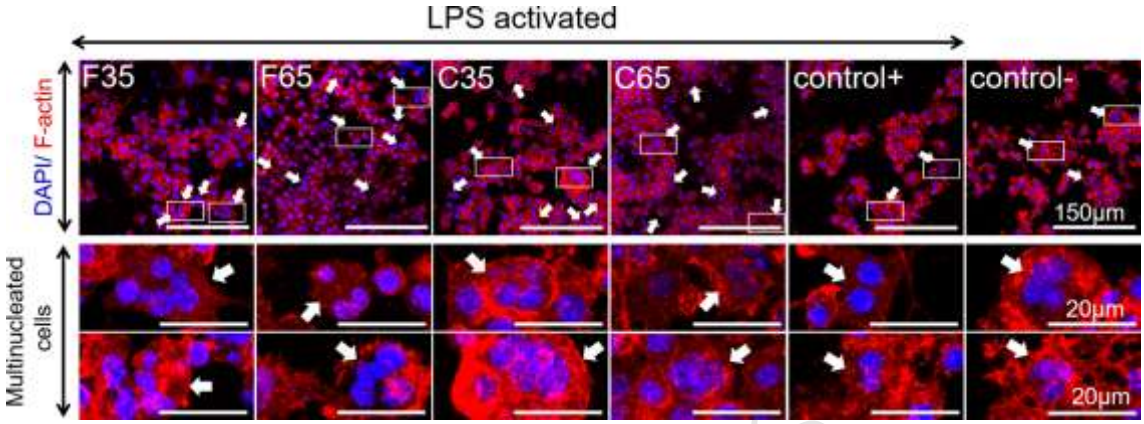

Supplementary Figure 8. *Presence of multinucleated cells (white arrows) on nano- and microstructured hydroxyapatite 6 hours after LPS stimulation. Cells were stained for F-actin (red) and nuclei (blue). RAW cells seeded on glass coverslip were used as a control group. Control+ represents cells with LPS stimulation whilist control- cells without LPS stimulation. Scale denotes 150 µm and for magnified images 20 µm. The brightness and contrast of images was modified using Fiji/Image-J package.*

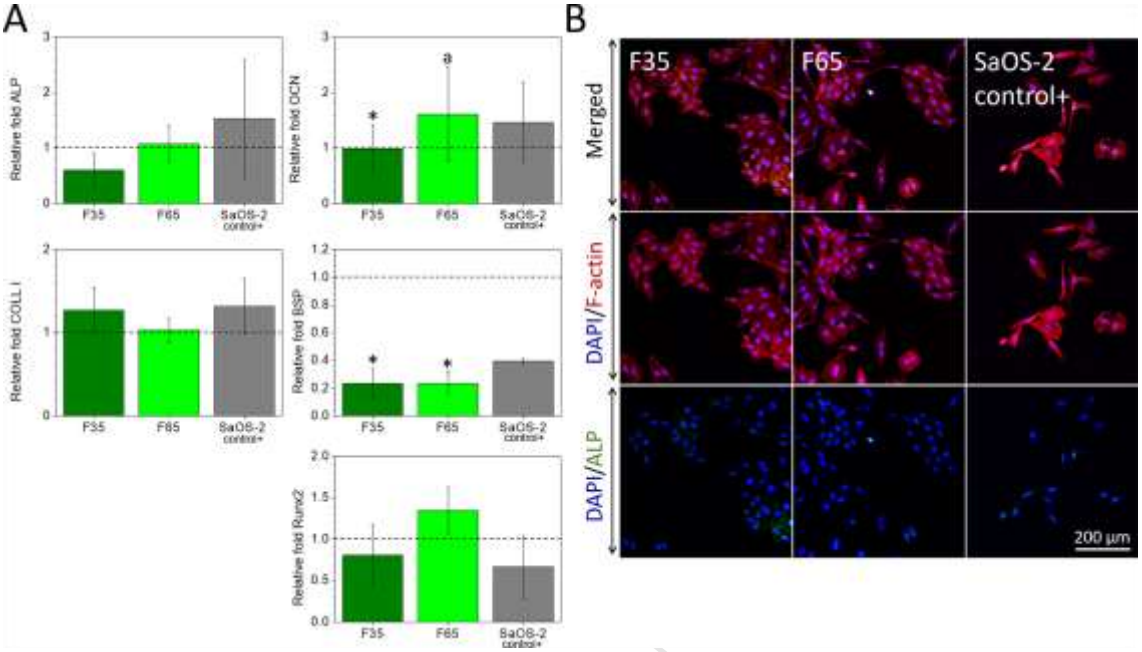

Supplementary Figure 9. *Effect of CDHA F- RAW conditioned medium, after induction with LPS, on osteogenic activity of SaOS-2.* **A)** *Relative expressions of osteogenesis related genes: ALP, Runx2, BSP, COLL I, OCN. * and a indicate statistically significant differences (P < 0.05) compared to the SaOS-2 control+ and F35, respectively.* **B)** *Representative confocal images of SaOS-2 morphology after 3 days of exposure to CDHA F- RAW, after induction with LPS, conditioned medium. Cells were stained for F-actin (red), nuclei (blue) and ALP (green). Scale bar in all images denotes 200 µm. The brightness and contrast of images was modified using Fiji/Image-J package.*

GRAPHICAL ABSTRACT